

Design and Implementation of a Digital Control System for a Turbo-Generator

by

Student: Fadi Shakkour

FADSHAK001

SUBMITTED TO THE UNIVERSITY OF CAPE TOWN

In fulfillment of the requirements for the degree

Master's of Science in Engineering

Faculty Engineering and the Built Environment

Electrical Engineering Department

UNIVERSITY OF CAPE TOWN

Date of submission:

Supervisors:

Professor Edward Boje

UCT Electrical Engineering

Professor Eduard Eitelberg

OBC Electrical Engineering

The copyright of this thesis vests in the author. No quotation from it or information derived from it is to be published without full acknowledgement of the source. The thesis is to be used for private study or non-commercial research purposes only.

Published by the University of Cape Town (UCT) in terms of the non-exclusive license granted to UCT by the author.

DECLARATION

I, Fadi Shakkour, hereby declare that the work on which this dissertation/thesis is based is my original work (except where acknowledgments indicate otherwise) and that neither the whole work nor any part of it has been, is being, or is to be submitted for another degree in this or any other university.

I empower the university to reproduce for the purpose of research either the whole or any portion of the contents in any manner whatsoever.

Signed by candidate

Signature:

Date:30/10/2023.....

Acknowledgment:

First and foremost, I am extremely grateful supervisors, Prof. Edward Boje and Prof. Eduard Eitelberg for their invaluable advice, continuous support, and patience during my M.Sc. study. Their immense knowledge and plentiful experience have encouraged me in all the time of my academic research and daily life.

I would like also to appreciate all the support I received from ORT Braude College, may it be from my colleagues or the management.

Also, I would like to express my gratitude to my wife, my parents, my siblings, and family. Without their tremendous understanding and encouragement in the past few years, it would be impossible for me to complete my studies.

Abstract:

Laboratory turbo generators are systems that help to give a better understanding of the concept of a real power plant based on a turbo generation. They are built to have flexibility in some parameters, such as different fuels, different temperatures, fuel consumption, etc. This flexibility leads to each turbine being entirely unique. Thus, it becomes difficult to apply the regular models which are taught in literature, to control the outputs or predict the behavior of the turbines.

This dissertation studies the behavior of the laboratory turbo generator located in ORT Braude College, according to inputs of fuel consumption and excitation voltage on the rotor, compared to the outputs of frequency and voltage on the load. This specific turbo generator is a twin-shaft generator, which means that it is used for wide range of output frequency, which is the opposite of traditional power plant requirements. From initial measurements, it was deduced that the system is an inherently unstable open-loop system for a wide range of frequencies which are available for the generator, between 1000 RPM and 8000 RPM. By using the Bristol gain numbers, it was shown that no controller may be designed to regulate both outputs independently by the given inputs for the system, as it requires a larger scope of the input than the system is physically able to give.

The author proceeded by deeper analysis of the system, to model the turbo generator and have a better understanding of the connection between the inputs and outputs, to do so the connection between Bristol gains and quantitative feedback theory is achieved. The analysis started by laws of energy conservation, then to include experimental data to understand the connection between energy, efficiency, magnetic flux, fuel flow and excitation voltage and how they are connected to the rotation of the rotor in the generator. It was shown using Bristol gains that, unlike in power plants, the efficiency is strongly connected to the speed of the generator shaft, and proved again how, for this system, it is physically impossible to design a 2×2 controller and gave a better understanding for choice of input-output pairing due to weak coupling. As a conclusion from this analysis, a single SISO (single input single output) digital controller was designed, where the load frequency is controlled by the excitation voltage, which is the opposite of how a conventional power plant is controlled. The author uses a proportional and international controller by using “Ed’s PI controller” (Professor Eduard Eitelberg) to overcome possible issues in the integration part.

The controller was designed using the analysis of the turbine by implementing it in MATLAB, to have an initial theoretical digital proportional-integral controller and test it in a simulation using Simulink-MATLAB. The final step was to implement the controller through a micro-controller (teensy3.6) to do the calculations using software. The usage of a micro-controller requires an interface between it and the turbo generator as they work on different range of voltages. To overcome the difference in voltages, the author designed and implemented electronic circuits on the one hand to reduce the generator’s output voltage as well as filtering noise from the signal, then the micro-controller can measure the frequency. On the other hand, another circuit to amplify the voltage output from the micro controller and to the excitor of the generator’s rotor. While the implemented controller validated the theoretical model, there is a need for further investigation of the non-linearity in the system since the generator produces limit cycle oscillations.

Table of Contents

Abbreviations	1
Chapter 1 Introduction	1
1.1 Scope of study.....	1
1.2 Limitations	1
1.3 Report overview.....	1
1.4 Turbo generator.....	2
1.5 Problem statement.....	4
1.6 Objective of research	4
Chapter 2 Literature Review	5
2.1 Power system control and stability	5
2.1.1 Power system controllers	6
2.1.2 Generator Voltage equations.....	8
2.1.3 Generator Frequency Equations.....	8
2.1.4 Frequency Control.....	9
2.2 Models of Industrial Power plant Gas Turbo Generator.....	10
2.3 Conclusion	11
Chapter 3 Model description	12
3.1 Island Mode Power Plant	12
3.2 Multivariable Control Systems	13
3.2.1 Connection Between Bristol Gains and Quantitative Feedback	14
3.2.2 Considerate Control	15
3.3 Conclusion	17
Chapter 4 System Analysis	18
4.1 First runs and analysis of the system	18
4.2 Steady-state analysis and constraints	20
4.3 Analysis of the system	22
4.3.1 Energy balance in turbogenerators.....	23
4.3.2 A turbo-generator in island mode.	23
4.3.3 Experimental turbo generator in island mode	25
4.3.4 Linearized model for experimental turbo-generator	32
4.3.5 Choice of input output pairing for experimental turbo-generator	35
4.4 Conclusions.....	36

Chapter 5 Theoretical Design	37
5.1 Controller design.....	37
5.2 Controller implementation simulation	43
5.3 Simulation results.....	44
5.4 Conclusions.....	46
Chapter 6 Controller implementation.....	47
6.1 Hardware implementation.....	47
6.1.1 Measuring the load’s frequency	47
6.1.2 Frequency measurement circuit design.....	48
6.1.3 Regulating the generator’s excitation voltage.....	50
6.1.4 Regulating the generator’s excitation voltage circuit design	50
6.2 Software implementation	51
6.2.1 Frequency measurement of the generator signal.....	51
6.2.2 Frequency measurement of the generator signal.....	52
6.2.3 User input to control parameters	52
6.2.4 Data logging.....	53
6.3 Disturbances creation.....	53
Chapter 7 Practical Aspects and Results	54
7.1 Frequency control results in a closed-loop system.	54
7.2 limit cycle comparison between experimental results and simulation.....	56
7.3 conclusion	58
Chapter 8 Conclusion.....	59

Abbreviations

AC	Alternative Current
ADC	Analog to Digital Converter
AGC	Automatic Generation Control
APU	Auxiliary Power Unit
DC	Direct Current
EoM	Equation of Motion
IEC	Israel Electric Corporation
LHP	Left Half Plane
LPF	low-Pass Filter
MMF	Magneto Motive Force
OBC	ORT Braude College
Op-Amp	Operational Amplifier
PAM	Pulse-Amplitude Modulation
PI	Proportional and Integral
PMW	Pulse-Width Modulation
RHP	Right Half Plane
SPS	Stand-alone Power System

Chapter 1

Introduction

The physical object of the research is a “Gas Turbine Electrical Generation System” from Turbine Technology company, in the USA[1]. The TurboGen module used for this project is a jet engine powered electrical generation system. The module is designed expressly for engineering education and research purposes mainly for thermodynamic experiments.

1.1 Scope of study

This master’s dissertation utilizes an existing turbo-generator that produces 3-phase electrical energy which has basic manual levers for controlling the inputs. The system in question is designed for thermodynamic laboratory experiments to test various variables, such as energy transfer, atmospheric pressure effects on the fuel, etc. The design process is documented in the form of this dissertation and is presented to record the decisions, trade-offs and attempts made in producing a working automatic digital controller prototype. This will answer questions regarding the complexity and feasibility of the implementation of such automated system.

The turbo-gen system was tested manually to demonstrate the actual load frequency functions since the manual system did not behave according to theoretical models taught in literature. Thus, there was a need to study the behavior of the turbo-gen system manually, create a theoretical model, then build a special algorithm and implement a digital controller to meet the actual specifications of the turbo-generator.

The automated system was successfully operated at a frequency close to 400 Hz. During these trials, the turbines suffered some damage, likely due to overheating. Unfortunately, the turbo-generator is no longer operational, as it shuts down automatically within a few seconds starting it up. Further testing of the designed PI control system is not possible in the near future. Fortunately, we have recorded enough data to prove the design concept.

1.2 Limitations

This study is limited to the design of the digital control and the prototyping and testing for a specific laboratory turbo-generator. This study does not extend into the development of a general model or control for autonomous power-plant control of a turbo-generator.

1.3 Report overview

The documentation includes the following chapters:

1. Introduction, this chapter, a presentation of the broad context of this dissertation.
2. An overview of the current state of the art in turbo-generators.
3. System analysis of the presented turbo-generator.
4. Theoretical design of the controller.
5. Hardware and software digital controller implementation.
6. Practical aspects and results of the controller.
7. The report concludes with an evaluation of the system as built.

1.4 Turbo generator

Traditionally, the bulk of electricity was generated by steam-turbine and three-phase generator units on a single axis. Steam can be obtained either from geo-thermal wells (as in Iceland), or generated in fossil-fuel fired boilers, or in nuclear power plants. All such power plants require massive capital investment prior to the sale of power to users. This presents a barrier to entry into the energy market for medium and small companies. Fossil-fired and nuclear plants are not suitable for frequent start-up – they are used to cover the base load and the scheduled load changes. Neither is particularly suitable for meeting the unanticipated rapid (e.g. hourly) changes in the energy demand.

The politically very popular wind and solar power generators have the problem of not necessarily being available when there is demand – until suitable energy storage technology becomes available, or when sufficient numbers of 'alternative' generators are interconnected over many time-zones. A significant amount of hydro-energy is available only in a few wet countries of the world.

Reciprocating internal combustion engines are used for small-scale electricity generation. However, industrial-scale generation is based on gas-fired turbines, the utilized 'gas' may be atomized and evaporated liquid fuel. Relative to the conventional steam-turbine generating units, the gas-fired turbo-generators require less initial capital investment and they can be started up on a short notice. Yet, gas-fired turbo-generators operating costs, however, are much higher, they have been used to cover peak demand, which is by definition of relatively short duration.

To put things into perspective, in South Africa, the peaking power stations are hydroelectric, hydro-pumped and gas turbine stations. According to Eskom [31], there are fourteen peaking power stations with a total nominal capacity of 5894.4 MW's.

An exception to this paradigm, in Israel about 50% of the entire energy supply is from gas-fired turbo-generation while coal-fired steam turbines supply the other half. In installed capacity, the ratio is two-to-one in favor of the gas-fired turbines – 5 GW of coal-fired steam units, 10 GW of gas turbines, and 1 GW of diesel fired turbines for peak load [32]. The majority of Israeli turbo-generators are actually quite large and rotate at 3000 RPM or slower. They generate 50 Hz electrical power in three-phase generators that sit on the same shaft as the turbine and compressor.

It seems that most emergency and other relatively small gas-fired turbines rotate at speeds that are not suitable for 50 Hz power generation. In the case of turbines which rotate at a high speed, the turbine shaft is connected mechanically to the generator shaft through a speed-reducing gearbox. While an interesting idea, using the thrust of a fast-rotating turbine's exhaust – or the high-pressure air bled off from the turbine inlet – to drive a slowly rotating turbine-generator unit does not seem to be popular in ground-based power generation.

Indirect coupling, however, can be found in aircraft 400 Hz power generation systems – and such a turbo-generator is operated in the Electrical and Electronic Engineering Department of ORT Braude College (OBC). Its operation is illustrated in Figure 1. The turbo-generator – as built by Turbine Technologies Ltd – is shown schematically in Figure 1.1 of the TurboGen™ Operator's Manual. Its reproduction here is permitted by the academic study-related exclusion clause in the copyright note of Turbine Technologies Ltd on page *i* of this manual.

Ordinary discussions of electricity production refer to the electrical grid, where there will be numerous generators, with each generator affecting the other, and there will be converters from high voltage produced by the power plants to lower voltage and so on and so forth. However, for this study is on another aspect of electricity generation, namely "Island mode" or "Standalone mode". As the second name implies, the

turbine we are using is not connected to a grid, as though it is supplying power to an island, and is the only power plant on the island present.

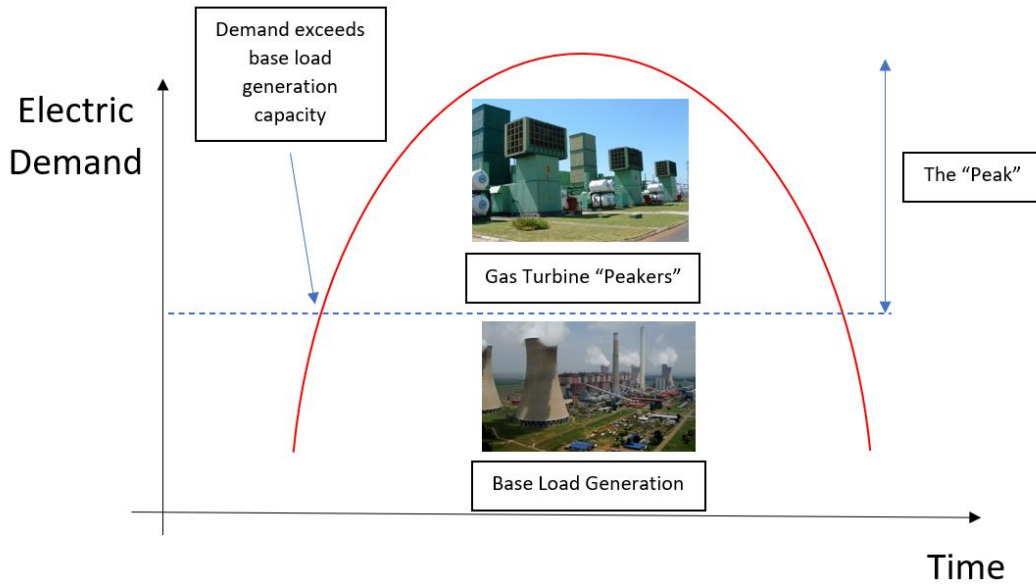


Figure 1.1: Electrical power demand curve. [1]

The system is composed out of two main parts: the engine and the generator, as seen in the following figure:

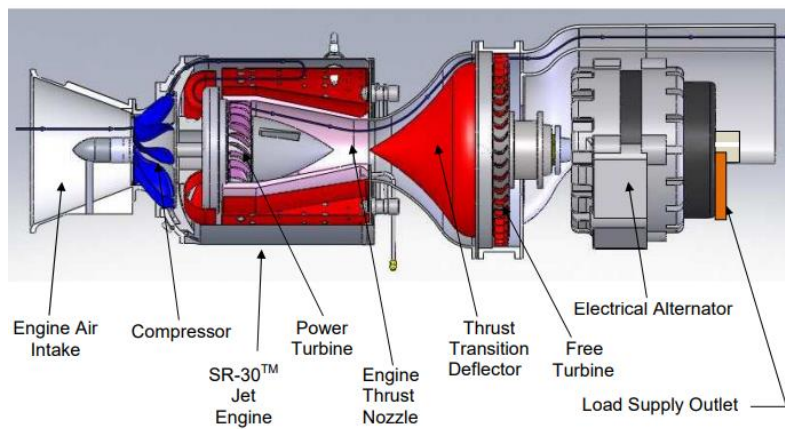


Figure 1.2: Sketch of the "Gas Turbine Electrical Generation System". [1]

Engine: A pure turbojet, the engine is representative of all straight single stage jet engines in which combustion results in an expanding gas that is sufficiently capable of producing useful work and propulsive thrust. Consisting of a centrifugal flow compressor, annular combustor, and axial flow power turbine, the engine is typical of the basic engine core found in turbofan, turboprop, and turboshaft gas turbine engines. These types of engines are used for aircraft, defense systems, and maritime propulsion as well as stationary and industrial power generation. The engine is fueled with A1 aircraft-grade diesel. It starts up by using an external compressor that pushes air and starts rotating the turbine. After the turbine reaches a certain RPM,

it ignites the fuel and shuts down the air supply from the compressor. During operation the turbine (as all jet engines) continues working without any external help. The user is able to control how much fuel the turbine consumes using a throttle lever. Fuel is provided to the atomization nozzles via the fuel controller. The engine speed is regulated by controlling the amount of fuel entering the combustor through the fuel atomization nozzles. Fuel is delivered to the controller at constant pressure. The controller then regulates the amount of fuel reaching the atomization nozzles through a high pressure, return flow throttling technique. At low engine speeds, the majority of fuel entering the fuel controller is allowed to return to the fuel source. When higher engine speeds are desired, the fuel controller return line is restricted causing more fuel to reach the nozzles. The engine is fully throttleable over the entire performance envelope from idle to maximum power. There is no restriction on the speed or rate at which the fuel controller may be moved. The fuel controller movement causes a nearly instantaneous response in engine power.

Turbo-generator: A free turbine-driven electrical turbo-generator; it is representative of almost any electrical generation station where a prime mover spins an alternator to generate electricity. In the case of TurboGen, the thrust from the jet engine is ducted to a second stage axial flow turbine wheel, turning that turbine by thrust force only (no directly connected shaft, meaning not mechanically connected to the engine, only thermodynamically connected). A free turbine is defined as a turbine that is not directly linked to a power source by a drive shaft, but rather is driven thermodynamically by hot gases rushing through the system. The power delivered is related to the pressure difference and the mass flow rate. That second stage turbine wheel is directly connected by a shaft to the electric alternator, causing it to spin and generate electricity. The TurboGen thus acts like a typical Auxiliary Power Unit (APU) (seen powering aircraft accessories while the main engines are shut down), or like an Electric Generation Peaking Plant (which is used to supplement baseload electric generation plants on days where demand exceeds supply). The synchronous turbo-generator in use has 12 poles and is connected to a three-phase load. The user is able to control the excitation current in the rotor coil by the excitation load lever. If desired, this load lever gives the operator the capability to direct a variable excitation current to the turbo-generator to provide variable loading on the generator system. Although it is commonly defined as excitation current, this system controls the excitation voltage with the lever. In the experimental set-up, the generated electricity is connected to a Y-connected load, resistive only, and there is no inductive or capacitive load.

1.5 Problem statement

While the system used for this dissertation is originally meant for thermodynamic experiments, it uses the generator mainly for calculation of many thermodynamic parameters such as how much energy is produced by the fuel, what is efficiency and how the temperature of the system affects its behavior. Even though the 3-phase generator has a range between 15 Hz and 1 kHz (electrical frequency generated), the generator becomes unstable when it goes above 100 Hz. When taking into consideration the power delivered to the load, the turbo-gen module must include the reactance which increases as the frequency increases. Yet the research purpose regards the frequency stability and not voltage (power) stability and delivery.

1.6 Objective of research

The objective of the research is to analyze the TurboGen[1] in OBC and to implement a digital controller that would stabilize the turbo-generator in the unstable range between 100 and 400 Hz, and also to give the user the ability to control it in various ways. It will be shown later in this dissertation that due to the nature of this turbo-generator, the frequency can be stabilized only by using one of the inputs, although the system has two inputs. The controller designed by the author will also open the possibility of performing other experiments using the system.

Chapter 2

Literature Review

In this chapter, information is found to provide a theoretical base for this study in the field of power generation control and stability, multi-loop control theory, and digital control. This information provides the reader with the knowledge needed for the research and development presented in the following chapters.

2.1 Power system control and stability

These days, as it has been for many decades, power plants are used to convert mechanical energy to electrical energy. These power plants need to be controlled in order to overcome any disturbance they encounter and regain steady-state condition. Among these disturbances are faults, load changes, line outages, and more. Power system stability, as mentioned in the IEEE[6], is the ability to regain a state of equilibrium after being subjected to physical disturbance, for a given initial operating condition. Power system stability may be classified into rotor angle, voltage, and frequency stability[2]. Each of these three stabilities can be further classified into sub-categories as in the following figure:

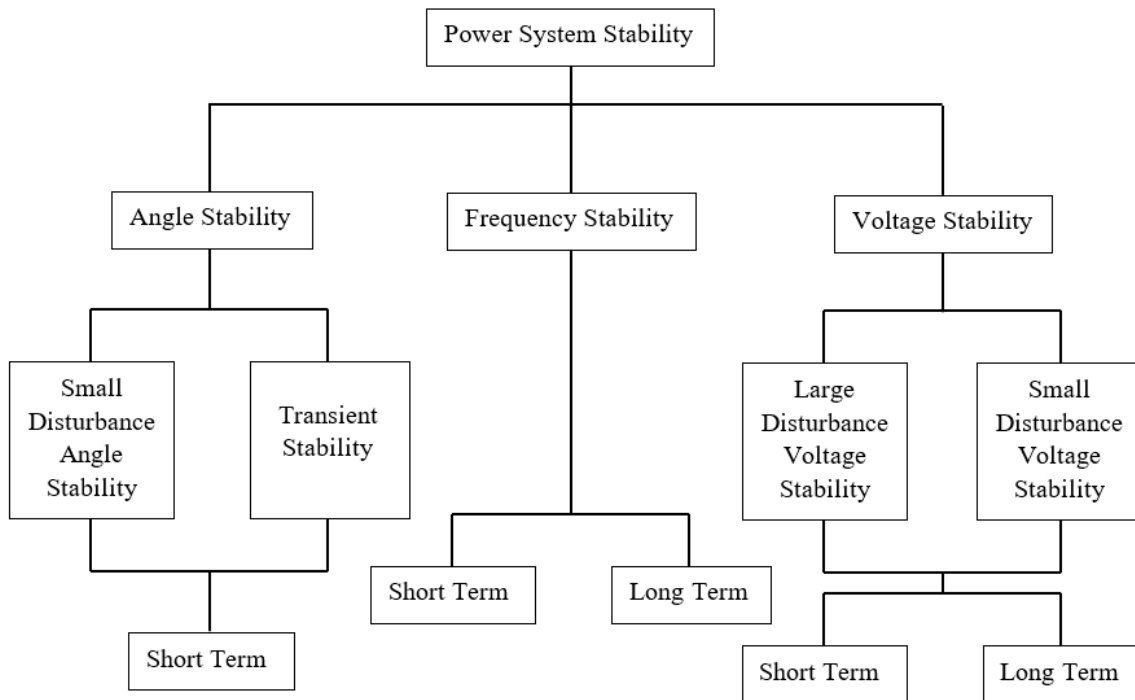


Figure 2.1: power system stability classifications[2]

The “Angle Stability” which is also referred to as “Rotor Angle Stability” refers to the ability to remain in synchronism when subjected to a disturbance, or in other words means that all the generators' electromagnetic torque is exactly equal to the mechanical torque in the opposite direction. If in a generator the balance between electromagnetic and mechanical torque is disturbed, due to disturbances in the system, then this will lead to oscillations in the rotor angle. With that being said

the turbo-generator that is used in this research is a stand-alone power plant, and thus there is no need for such stability or any subcategories thereof.

“Voltage stability” refers to the ability of a power system to maintain steady voltages at all buses in the system after being subjected to a disturbance. It depends on the ability to maintain/restore equilibrium between load demand and load supply from the power system. Instability occurs in the form of a progressive fall or rise of voltages of some buses. In voltage stability of the study, the period of interest may extend from a few seconds to tens of minutes. Thus, “Voltage Stability” may be a short-term or a long-term phenomenon.

The sub-category “Large Disturbance Voltage Stability” refers to the system's ability to maintain steady voltages following large disturbances such as system faults, loss of generation, or circuit contingencies.

The sub-category “Small-disturbance voltage stability” refers to the system’s ability to maintain steady voltages when subjected to small perturbations such as incremental changes in system load.

“Frequency Stability” refers to the ability of a power system to maintain steady frequency following a severe disturbance between generation and load. It depends on the ability to restore equilibrium between system generation and load, with minimum loss of load. Instability occurs in the form of sustained frequency swings leading to tripping of generating units and/or loads. The characteristic times of the processes and devices that are activated during frequency excursions will range from fractions of seconds to several minutes. Thus, “Frequency Stability” may be a short-term or a long-term phenomenon.

In this dissertation, the turbo generator used for this research has two levers that enable manual control of the fuel flow going into the engine of the turbine and excitation voltage that increases or decreases the electromagnetic load on the generator shaft/rotor. The author did investigate voltage and frequency stability for the studied turbine, and it will be shown that for this turbo generator only one output can be controlled independently, either load voltage or load frequency.

2.1.1 Power system controllers

In real power plants, there are several levels of controls involving a complex array of devices that are used to meet the requirements such as constant frequency and constant voltage. In a power system, there are controllers operating directly on individual system elements. In a generating unit these devices consist of prime mover controls and excitation controls. The prime mover controls are concerned with speed regulation and energy supply system variables such as boiler pressure, temperature, and flow. The function of excitation control is to regulate generator voltage and reactive power output. The desired MW outputs of the individual generating units are determined by the system-generation control.

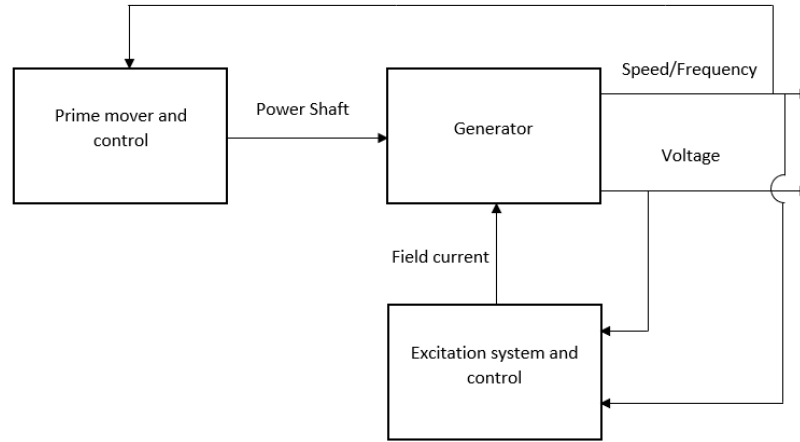


Figure 2.2: Power system and associated controls [2]

Usually, when mentioning the control systems for a generator/power system, there are two names for the controllers:

Automatic Voltage Regulation or AVR: the controller for the excitor to regulate the output voltage.

Turbine/Speed Governor: the controller for regulating the output frequency.

The output of the excitation system is the generator field voltage/current E_{fd} . The prime mover output is the mechanical torque T_m . The generator output is voltage (also called the generator terminal voltage) is V and frequency/speed is ω .

We will be focusing more on the linearized model of the turbine as it is useful for small signal analysis even though the generator is a non-linear device[2]. While there is a difference between the linearized model and the non-linear device. These differences may be dealt with after implementing the controller by fine tuning the controller's parameters. One of the philosophies in control engineering is to start with the linearized model, design the controller and continue to simulate the non-linear system to tune the controller[14].

Thus, the linearized model is as follows:

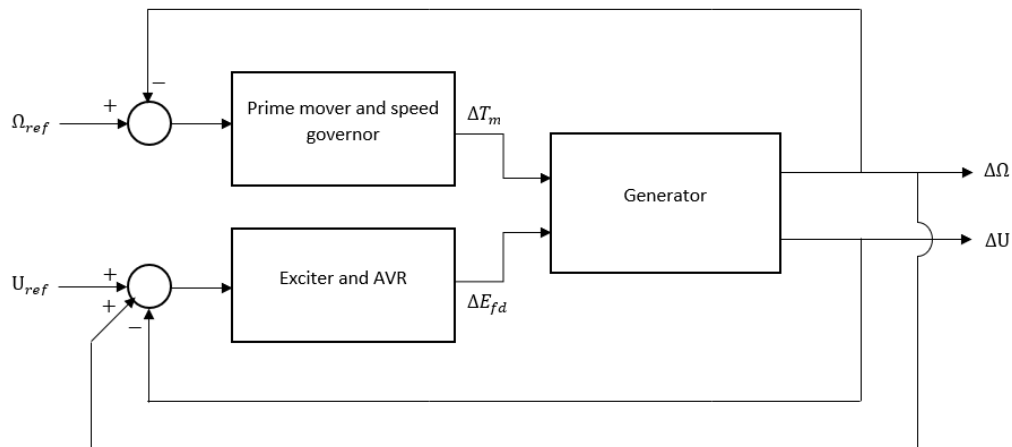


Figure 2.3: Linearized model of power system and associated controls [3]

2.1.2 Generator Voltage equations

A synchronous' stator and rotor may be defined using axes:

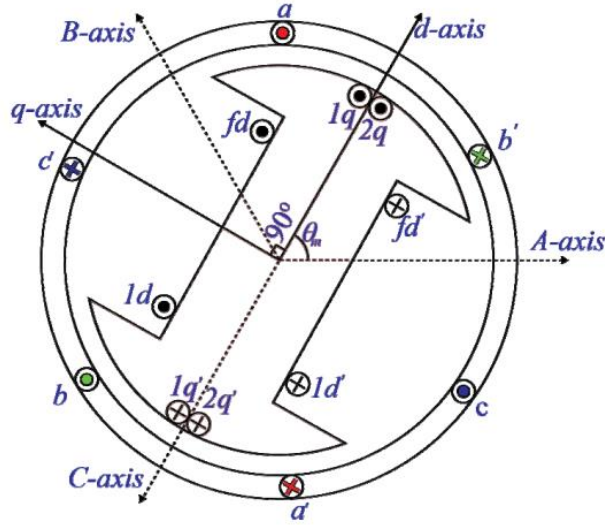


Figure 2.4: synchronous machine sectional view.[2]

The conductors a and a' represent the sectional view of one turn of the a-phase stator winding. By applying the right-hand rule at the conductor, it can be observed that the magnetomotive force (MMF) due to the conductors a and a' lie along axis marked A-axis. Similarly, the MMF due to b,b' and c,c' lie along B and C axis, respectively. The rotor field is excited by a DC voltage represented as v_{fd} with a field current i_{fd} . The MMF generated by the rotor field excitation lies normal to the pole surface, along the direct axis or d-axis. The axis in quadrature (leading or lagging by 90°) with respect to the d-axis is called the quadrature axis or q-axis. The q-axis can either be represented as a leading d-axis or lagging d-axis.

In power systems control, assuming the exciter input is based on the dq-axis machine representation, assuming the q-axis lags the d-axis, and adopting generating sign convention, the per unit (PU) stator terminal voltage U , is given by:

$$U = e_d + j e_q e_d = \frac{d\Psi_d}{dt} + \Omega\Psi_q - R_a i_d e_q = \frac{d\Psi_q}{dt} - \Omega\Psi_d - R_a i_q \quad (2.1)$$

e_d and e_q are the d-axis and q-axis components of the terminal voltage. Ψ_d and Ψ_q are the d-axis and q-axis components of stator flux linkage. i_d and i_q are the d-axis and q-axis components of stator current. Finally, R_a is the stator resistance.

In equation (2.1), $d\Psi_d/dt$ and $d\Psi_q/dt$ represent the voltages due to change in flux with time and are known as transformer voltages. These terms represent stator transients. The terms $\Omega\Psi_q$ and $\Omega\Psi_d$ are the speed voltages. The speed voltage terms represent the fact that after the transformation from stationary (abc) to rotating (dq) reference frame, a rotating flux wave will create speed voltages in the stationary armature. In stability studies[2], network transients are neglected because they are very fast. Therefore, the stator transients are also neglected.

2.1.3 Generator Frequency Equations

Power plants transform other sources of energy in the process of producing electrical energy. The generator is driven by a prime mover. From the viewpoint of frequency control, the power system

can be thought of as only one large power plant supplying one load. Two opposite torques act on the large rotating mass, namely a mechanical torque T_m and an electrical torque T_e . In case of an imbalance between these torques, the rotating mass will experience an angular acceleration or deceleration $d\omega/dt$ according to Newton's Second Law for rotating systems:

$$T_m - T_e = J \frac{d\Omega}{dt} \quad (2.2)$$

where J is the moment of inertia of the rotational mass. The inertia J has a stabilization effect, i.e., in case of an imbalance in torques, the frequency change is smaller for a system with high inertia compared to a system with low inertia, meaning that a high inertia system is slower.

Equation (2.2) is also known as the equation of motion (EoM). The equation of motion includes generally rotating components of the power system. We can notice that a sudden increase in the generation, namely in the mechanical torque, T_m , implies an increase in $d\Omega/dt$ and thus in the frequency in the system. Vice-versa, an increase in consumption, namely in the electrical torque T_e , implies a decrease in frequency. It is worth noting that the larger the inertia of the rotating mass is, the smaller the speed rate-of-change following a torque imbalance is.

The equation of motion can also be expressed in power terms by using the proportional relationship between power and torque:

$$P = T\Omega \quad (2.3)$$

By applying this relationship, the equation of motion in power terms (power balance equation) can be expressed as:

$$P_m - P_e = J\Omega \frac{d\Omega}{dt} = M \frac{d\Omega}{dt} \quad (2.4)$$

where P_m is the mechanical power, P_e is the electrical power and M is the angular momentum of a rotating system, defined as $M = J\Omega$. Although equation (2.4) does not include losses or efficiency, it will be shown below that both P_m and P_e are rotation speed dependent and will include efficiency, as well as how the imbalance will either cause the system to get to a steady rotational speed or cause it to accelerate until it automatically shuts down.

2.1.4 Frequency Control

Kundur discusses the theory of frequency stability [2]. He focuses on the determination of steady-state frequency which is determined by the characteristics of the load, the governors, and the Automatic Generation Control system (AGC).

Power system loads include a variety of electrical devices. The electrical power of some loads, such as lighting and heating loads, does not vary with frequency. The electrical power of motor loads does vary with frequency. The variation of the total load with frequency gives the power system a self-regulating characteristic, the electrical power of the load decreases/increases with a decrease/increase in frequency. The load's frequency-dependence dampens the response of frequency to disturbances. Typical values are 1-2 %, i.e., a 1 % change in frequency leads to a 1- 2% change in load.

2.2 Models of Industrial Power plant Gas Turbo Generator

Models of gas turbines can be categorized into low-power gas turbine, industrial power plant gas turbine (IPGT), and aero gas turbine models. In an IPGT, the mechanical power generated by the gas turbine can be used by an alternator to produce electrical power.

Najjar [26] investigated the performance of gas turbines in single-shaft and twin-shaft operation modes using a model of a free power gas turbine driving an electric dynamometer. GT operational data and their related curves for important parameters such as thermal efficiency, specific fuel consumption and net output power were considered in order to estimate GT performance. The results showed when the free power turbine engine was run in the single-shaft mode (especially with a low-speed ratio), the power was increased significantly (about 75% in the low-power region) at part loads. However, running the free power turbine engine in the two-shaft mode showed better torque characteristics at part load, which is important for transport applications and traction systems.

A model for a twin-shaft gas turbine was estimated by Hannett et al. [27]. They conducted a field-testing program to obtain the required data for simulation of the model and assessment of the gas turbine governor response to disturbances. During the process of model derivation, the model structure consisting of pertinent variables and parameters was determined. The researchers carefully considered steady-state characteristics of the gas turbine in order to capture dynamic responses of important variables including rapid load changes and load rejections. To adjust the model parameters, an intelligent trial and error process was employed until reasonable matches were obtained between tests and simulations. This methodology was the only practical procedure for the model derivation because of the nonlinearity of the process and its controls. The researchers had to provide the required performance data for each gas turbine component including the compressor, combustor, and turbines. Regardless of the complicated process of the model derivation, the resulting model could be useful for studies of system dynamics.

Yee et al. ([28],[29]) carried out a comparative analysis and overview of different existing models of power plant gas turbines. They identified, presented and discussed various kinds of gas turbine models in terms of their application, accuracy and complexity. They concluded from the research that despite their complexity, physical models are the most accurate and suitable for detailed study of the gas turbine dynamics. However, they stated that physical models are not appropriate for use in large power system studies. The researchers also indicated that for a more detailed analysis of power systems and their governors' behavior, the frequency-dependent model was the best choice. It was particularly useful in the case of weak coupling systems with large frequency variations.

Singh et al.[30] worked on the same system used in this dissertation. They presented a modern control-based system design approach for ensuring the stability and performance of the gas turbine engine, for various operation ranges. The primary objective of the control design was to compute the required fuel flow to the engine such that the shaft speed of the gas turbine engine tracks its commanded signal. The controller did assume that all states are measurable perfectly, which was not possible practically. Singh et al. focussed on controlling the engine shaft through the use of fuel flow, and there is a need to investigate the controller for the generator shaft, which is done in this dissertation.

2.3 Conclusion

Initially for this dissertation, there is a need to understand how the system works. this requires analysis and understanding the interaction between the loops, as there are two inputs which are fuel flow and excitation voltage, and two outputs which are frequency and supplied voltage.

Chapter 3

Model discription

In this chapter, information is found to provide the techniques that the author will be using, to enable analysis and implementation of the Turbo-Gen and control system in a digital form.

3.1 Island Mode Power Plant

In the field of power plant and electrical generation, it is more common to talk about a power plant that is connected to a grid. Through this connection, more power is produced so producers may provide the needed electricity for consumers. While power plants are connected to a grid there is a need for synchronization among power plants to keep steady operation.

“Island Mode” refers to the isolation of a power plant from the local electricity distribution network. This usually occurs after a major disturbance that may cause a shutdown of the power plant as a result of frequency and voltage excursions. While islanding, the power plant continues operating after disconnection from the grid. The disconnection from the power grid is initiated by the plant’s protection systems. Modern electrical grids often have features of an anti-islanding system using grid-interactive inverters as mentioned in IEEE standards [6]. Islanding the power plant enables it to re-stabilize and/or cool down without the penalty time of shutting down and starting again.

While the isolation for main power plants is to protect the power plant, mini-grid power systems may have either unintentional or intentional islanding. Unintentional islanding is done to protect the power plants as explained above. Intentional islanding is to provide electrical power for mini-grid customers. The Israel Electric Corporation (IEC) regulations [8], permit working in this “island mode” for personal usage, as they disconnect from the main grid in case of malfunction and supply their own power such as using solar panels.

“Island Mode” may also refer to a stand-alone power system (SPS), where there is no connection to the grid. SPS may vary by size, technology, and application. SPS electricity generation may vary as well. Some examples are photovoltaic systems for remote consumers that provide DC electricity but can also be converted to AC and diesel generators that provide AC with single-phase or 3-phase. An SPS is not necessarily built from one kind of electricity generation such as only photovoltaic systems, but can include multiple methods of electricity generation. In South Africa a stand-alone power system, requires the approval of the Planning and Building Development Management Department and other departments, but not from a city’s Electrical Service Department [34].

In this dissertation, although the Turbo-Gen is an experimental tool to simulate a gas power plant “Peaker” for grid purposes, it is nonetheless considered an SPS as there is no connection to anything but a resistive three-phase load. It will be shown that this kind of generator is not typical as its uncertainty in the plant changes a pole from the left half plane (LHP) to the right half plane (RHP) as the operational point changes, thus making the generator stable in some range of operation and unstable in the rest of the range. The author will explain how this phenomenon is investigated and how to stabilize the system.

3.2 Multivariable Control Systems

When it comes to multi-loop (multivariable processes) the industry usually starts the design for each desirable output y_i with a given input u_j , first by having all other loops open so there is no interaction between the loops whatsoever. After tuning the desired loop, the control engineer start closing the other loops, it can be one loop at a time or multiple at once, then tune in a recursive manner.

Eitleberg [23] explains, for a plant $\mathbf{P}(s)$ that needs n controllers $G_i(s)$ to regulate the outputs, if we take into consideration that there is only one loop closed and the rest are open, such as there are no interactions from the other regulators, then the loop transfer function will be:

$$L_{p_i}(s) = G_i(s)P_{ii}(s); i = 1, \dots, n \quad (3.1)$$

If any controller is activated by closing the other loops, then for the same input-output in the loop transfer function in equation (3.1) will change because of the interactions, given there are interactions. The new loop transfer function will be $L_i(s)$ for the same controller $G_i(s)$. One could work by closing each time one loop after the other, then tune them each time one more loop is closed, but Bristol suggested another way. He suggests that loop interactions should be measured by "... the ratio between two gains representing first the process gain in isolated loop and, second, the apparent process gain in the same loop when all other control loops are closed"[9].

Although Bristol gains [9] usually are considered at the beginning for the steady-state condition ($s = 0$ in the Laplace domain) to find how strong the interaction is, the more important part is the transfer function itself for all values of s , or at least in the frequency range of $0 \leq \omega < \omega_{gc}$, to ensure stability and meet the specifications of the design. One of the ways to calculate Bristol Gains is by using the Hadamard product, which is the element by element product between \mathbf{P} and the transpose of its inverse:

$$\mathbf{Y} = [Y_1 \dots Y_n]^T = \begin{bmatrix} P_{11} & \dots & P_{1n} \\ \vdots & \ddots & \vdots \\ P_{n1} & \dots & P_{nn} \end{bmatrix} [U_1 \dots U_n]^T = \mathbf{P}(s)\mathbf{U}(s) \quad (3.2)$$

$$\mathbf{B}(s) = \mathbf{P}(s) \circ [\mathbf{P}^{-1}(s)]^T \quad (3.3)$$

To measure the Bristol Gain of a certain row i and column j , meaning for input u_j and output y_i , there is no need to solve the whole matrix but:

$$B_{ij}(s) = \frac{P_{ij}(s) |\mathbf{P}_{(-j)(-i)}(s)| (-1)^{i+j}}{|\mathbf{P}(s)|} \quad (3.4)$$

The negative indices in equation (3.4) means the removal of the j^{th} row and the i^{th} column from the matrix $\mathbf{P}(s)$, meaning it is the determinant of the submatrix mentioned. For the sake of simplicity, after deciding pairs of input-output, the matrix $\mathbf{P}(s)$ will be reordered in such a manner that the input u_i will regulate y_i through using the controller $G_i(s)$. That way only the diagonal elements of $B_i(s)$ of $\mathbf{B}(s)$ are relevant.

$$B_{ii}(s) = \frac{P_{ii}(s) |\mathbf{P}_{(-i)(-i)}(s)|}{|\mathbf{P}(s)|} \quad (3.5)$$

Some of the Bristol Gains properties are as follows: First, the Bristol gains are calculated independently of the loops and loop designs. Second, the sum of all elements in a column or row inside the Bristol matrix would give the result of 1, in other words, $\sum_{i=1}^n B_{ij}(s) = \sum_{j=1}^n B_{ij}(s) = 1$. Third, in the case of $B_{ii}(s) = 1$ for $i = 1, \dots, n$, then the rest of the elements are zero, and we get independent loop designs of each and every loop. Finally, arguably the second most important aspect

of Bristol Gains, that large magnitude ratios B_{ij} are problematic. This will be further explained in section 3.2.2 in the explanation at equations (3.26) and (3.27).

3.2.1 Connection Between Bristol Gains and Quantitative Feedback

Comparing Bristol Gains to the Quantitative Feedback Theory[11], the author is using the Quantitative Feedback theory as means of better explaining the Bristol Gains. The loop transfer functions are defined at the beginning of the design as $L_{Qi}(s) = G_i(s)Q_i(s)$, where $Q_i(s) = 1/V_{ii}$ and $V(s) = P^{-1}(s)$. Thus, the Quantitative Feedback Theory is related to Bristol Gains as $L_{Qi}(s) = L_{P_i}(s)B_i^{-1}(s)$. yet both Quantitative Feedback Theory and Bristol Gains of these assume all other loops are regulated perfectly and that other loops are ideal such as the regulated outputs y_j ($j \neq i$) are independent of the input u_i .

So, for the consideration in equation (3.4), this loop is closed by using the controller G_i with L_{P_i} as defined in equation (3.1). Making the new controller matrix excluding G_i defined as $\mathbf{G}_{(-i)(-i)}$, the system without loop i is:

$$\mathbf{Y}_{(-i)}(s) = \mathbf{P}_{(-i)(-i)}(s)\mathbf{U}_{(-i)}(s) + \mathbf{P}_{(-i)i}(s)U_i(s) \quad (3.6)$$

$$\mathbf{U}_{(-i)}(s) = \mathbf{G}_{(-i)(-i)}(s)[\mathbf{R}_{(-i)}(s) - \mathbf{Y}_{(-i)}] \quad (3.7)$$

$$Y_i(s) = P_{ii}(s)U_i(s) + \mathbf{P}_{i(-i)}(s)\mathbf{U}_{(-i)}(s) \quad (3.8)$$

$$U_{(-i)}(s) = G_i(s)[R_i(s) - Y_i] \quad (3.9)$$

Looking at the whole system

$$\mathbf{L}(s) = \mathbf{P}(s)\mathbf{G}(s) \quad (3.10)$$

Thus, the other subsystem transfer function for diagonal \mathbf{G} is:

$$\mathbf{L}_{(-i)(-i)}(s) = \mathbf{P}_{(-i)(-i)}(s)\mathbf{G}_{(-i)(-i)}(s) \quad (3.11)$$

If we take a look only at the loop transfer function with the index i (diagonal element L_{ii}) while manipulating some of the equations above, it can be defined as:

$$L_i = L_{P_i} \left\{ 1 - \mathbf{P}_{i(-i)}\mathbf{P}_{(-i)(-i)}^{-1}[\mathbf{I} + \mathbf{L}_{(-i)(-i)}^{-1}]^{-1}P_{ii}^{-1}\mathbf{P}_{(-i)i} \right\} \quad (3.12)$$

The expression in equation (3.12) inside the braces is the inverse of the relative gain Λ_i of the loop.

$$\Lambda_i^{-1} = 1 - \mathbf{P}_{i(-i)}\mathbf{P}_{(-i)(-i)}^{-1}[\mathbf{I} + \mathbf{L}_{(-i)(-i)}^{-1}]^{-1}P_{ii}^{-1}\mathbf{P}_{(-i)i} \quad (3.13)$$

In the case of $\mathbf{L}_{(-i)(-i)}^{-1} \rightarrow 0$, the relative gain becomes the Bristol gain.

$$B_i^{-1} = \lim_{\mathbf{L}_{(-i)(-i)}^{-1} \rightarrow 0} \Lambda_i^{-1} = 1 - \mathbf{P}_{i(-i)}\mathbf{P}_{(-i)(-i)}^{-1}P_{ii}^{-1}\mathbf{P}_{(-i)i} \quad (3.14)$$

For this dissertation, it is sufficient to use the two inputs two outputs system, as the calculations are easier. As mentioned before, after allocating pairs of input-output, the two Bristol gains are equal according to the equation, yet the relative gains are not necessarily equal to equations (3.12) and (3.13):

$$B_1^{-1} = B_2^{-1} = B^{-1} = 1 - \frac{P_{12}P_{21}}{P_{11}P_{22}} \quad (3.15)$$

$$L_1 = L_{P_1} \Lambda_1^{-1} \quad \text{with} \quad \Lambda_1^{-1} = \frac{1 + L_{P_2} B^{-1}}{1 + L_{P_2}} = \frac{1 + L_{Q_2}}{1 + L_{P_2}} \quad (3.16)$$

$$L_2 = L_{P_2} \Lambda_2^{-1} \quad \text{with} \quad \Lambda_2^{-1} = \frac{1 + L_{P_1} B^{-1}}{1 + L_{P_1}} = \frac{1 + L_{Q_1}}{1 + L_{P_1}} \quad (3.17)$$

In the case of $B(s) = 1$, we get independent loop designs of $L_{P_1}(s)$ and $L_{P_2}(s)$, as a result from $\Lambda_1^{-1} = \Lambda_2^{-1} = 1$. Nonetheless, yet one cannot assume a case of $B(s) = 1$, or to say that in steady state $B(0) = 1$ is sufficient.

3.2.2 Considerate Control

In the multivariable control field, we already discussed how the interactions between inputs may affect each output and how to approach it, but as Eitelberg [24] mentioned “Successful persons activate available resources to achieve their intended goals. Wise persons also consider unintended consequences. The same applies to control system design...”. Thus, if we look at the output Y_i and we want to change it, usually we would modify the corresponding input U_j that was paired to it. In this section we are not going to assume that the input-out pairs have the same indices. Inconsiderate control means using only the paired input U_j to change the output Y_i but without changing the value of other inputs $U_i = 0, i \neq j$. This kind of change in the inputs will change the output Y_i as intended but will result in deviations Δ of all other outputs, which may be called 'unintended' consequences:

$$\mathbf{Y} = [\Delta Y_1 \dots Y_i \dots \Delta Y_n]^T = [P_{1j} \dots P_{ij} \dots P_{nj}]^T U_j \quad (3.18)$$

If the scope of change in input U_j causes marginal deviations on the other outputs from a low interaction behavior in the system, we can ignore this problem. To solve this problem, we should also modify $U_i = 0, i \neq j$ according to the change in the main input U_j so it only affects the output Y_i . This is defined as considerate control, changing the output Y_i through the input U_{cj} with a combination of in the other inputs to minimize the other outputs' deviations. At first, we require that all elements in the output vector \mathbf{Y}_c be equal to zero except the output with the index i as follows: $\mathbf{Y}_c = [0 \dots 0 Y_{ci} 0 \dots 0]^T$. In order to calculate the deviations in all other inputs, we will calculate beforehand the inverse matrix of the system:

$$\mathbf{V}(s) = \mathbf{P}^{-1}(s) = [V_{ij}(s)] \quad (3.19)$$

$[V_{ij}(s)]$ is a square matrix with n rows and n columns. The considerate input vector is therefore defined as:

$$\mathbf{U}_c = [\Delta U_{c1} \dots U_{cj} \dots \Delta U_{cn}]^T = [V_{1i} \dots V_{ji} \dots V_{ni}]^T Y_{ci} \quad (3.20)$$

This kind of method might be called 'hijacking' all inputs to change one output. Yet, at the same time we obtain considerate control to not affect any other output. We can describe all inputs by the following equation:

$$\mathbf{U}_c = \mathbf{P}^{-1} \mathbf{Y}_c \quad (3.21)$$

This kind of feed-forward is usually not implementable. For this control to be considerate only the ratios in equation (3.20) must remain. That way we can calculate the modification of all inputs by using the ratios between them and the input U_{cj} :

$$\Delta U_{ck} = \frac{V_{ki}}{V_{ji}} U_{cj}, \quad k = 1, \dots, n; k \neq j \quad (3.22)$$

This kind of implementation is a feed-forward for the output Y_i , though as above it may be not implementable as it may be non-causal or improper. To try and implement it, one possibility is to insert a filter for all inputs as follows:

$$\Delta U_{ck} = \left[\frac{V_{ki}}{V_{ji}} F_{cj} \right] \left(\frac{1}{F_{cj}} U_{cj} \right), \quad k = 1, \dots, n; k \neq j \quad (3.23)$$

However, F_{cj} must be designed to allow $(V_{ki}/V_{ji})F_{cj}$ to be implementable for each and every k and to define a new input as $U_{cj}^F = U_{cj}/F_{cj}$. Nonetheless, it must always be kept in mind the range of the outputs that are expected as well as the range of the input values to achieve them. If we look at the case where input ranges are independent of the manner in which the outputs are controlled, then the inputs become considerate inputs $U_{cj} = U_j$, meaning if we take the inputs as considerate inputs then the output become a considerate output as well, and we get the following from comparing equation (3.18) with (3.20)

$$Y_i = (P_{ij}V_{ji})Y_{ci} \quad (3.24)$$

Equation (3.24) can be written as the ratio of the achievable ranges of inconsiderately and considerately controlled output number i is:

$$\frac{Y_i}{Y_{ci}} = (P_{ij}V_{ji}) \quad (3.25)$$

On the other hand, if the plant output range must be achieved under both control frameworks, then the input actuator ranges must be modified, and we then require $Y_{cj} = Y_j$. This time if we compare equations (3.18) and (3.20) we get the result:

$$U_{cj} = (V_{ji}P_{ij})U_c \quad (3.26)$$

Again, the ratio of the required input ranges for considerately and inconsiderately controlled output number i is:

$$\frac{U_{cj}}{U_j} = (P_{ij}V_{ji}) \quad (3.27)$$

As seen, both ratios in equations (3.25) and (3.27) are equal, and more precise they are the Bristol gain of $B_{ij} = P_{ij}V_{ji}$. From this, we can deduce that if the Bristol gain has a large magnitude, it might cause a problem, as the considerate control of Y_i using U_j either demands increasing the input by that value or decreasing the output scope. Also, from the Bristol gains we can calculate:

$$\frac{V_{ki}(s)}{V_{ji}(s)} = \frac{B_{ik}(s) P_{ij}(s)}{B_{ij}(s) P_{ik}(s)} \quad (3.28)$$

And then calculate the inputs as:

$$U_{ck} = \frac{B_{ik}(s) P_{ij}(s)}{B_{ij}(s) P_{ik}(s)} U_{cj}, \quad k = 1, \dots, n \quad (3.29)$$

So, we may implement the considerate control either using feed-forward by calculating and coordinating the inputs to change some outputs without changing the others based on the certainty of the plant, thus the uncertainty may lead to fine tune because of the change in the calculation, yet this method work if the uncertainty is neglectable. Or we may implement the considerate control by feedback.

This kind of control helps to coordinate the inputs for regulating the output. This publication does not take into consideration the uncertainty and it seems that there is no simple way to take include such considerations.

Boje [3] has examined the application of QFT to design a 2×2 system for a power system, where the inputs are mechanical torque and generator field voltage, and the outputs are frequency and supplied voltage. Boje invalidates the approach that each paired input-output may be designed as an independent SISO system, arising from the assumption that frequency and terminal voltage are decoupled. Boje also designs a forward path decoupler to reduce the interaction between the loops. Thus, Boje's approach is close to Eitelberg's [24], except for his use of Perron root-based interaction measure to reduce the interaction.

3.3 Conclusion

The Bristol Gains understanding would enable the author to analysis of the input-output pairs are, as mentioned in section 2.1.1, to see how string is the connection between the two loops. Then the system must then be simulated in MATLAB in order to know what kind of controller will be used, how the digital implementation will affect the system and what to expect of the closed loop system. Last but not least, implement the controller, and compare performance between the simulated and real-time controller.

Chapter 4

System Analysis

Initially, the project aimed at designing a 2×2 digital control system. The two available inputs are the fuel flow and excitation voltage. The intended outputs were voltage and frequency – on the load. As an example: the system would have been a standalone power plant in the island-mode with 3 phase-load. So according to the requirement of the clients, the controller should manipulate the inputs to get a steady voltage and frequency. The disturbance in the whole network will be from the changes in the load, as an increase in the resistive load would decrease the electromagnetic load on the rotor and vice versa.

4.1 First runs and analysis of the system

Prior to starting the design of the controller, we needed to understand the system physically and model it mathematically. This included knowing the system's limitations so that we did not damage it. Analyzing the system as a whole does not mean only to have step response and have its mathematical model, it also means comprehending every aspect of it. For example, how changing one of either input (excitation and fuel flow levers) changes the outputs (load voltage and frequency) in the system. The data collected for the following analysis is collected from the data logging system installed in Turb-Gen from the manufacturer. During our first trials, we noticed several things – some of them are not mentioned in the manual:

- 1) The change in fuel flow leads to a near-instantaneous change in the jet engine RPM, but to a more gradual change in the turbo-generator RPM.

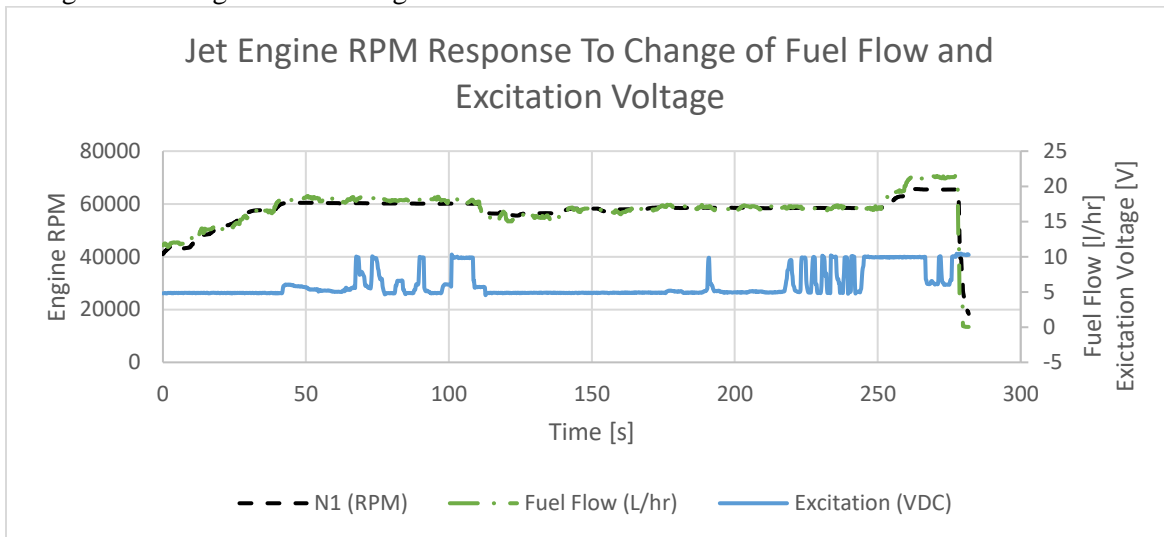


Figure 4.1: Jet engine RPM response to change in fuel flow and excitation voltage. Black line (dashed line): jet engine RPM. Green line (dash-dotted): fuel flow rate. Blue line (solid line): excitation voltage. x-axis is in seconds.

Figure 4.1 shows that both lines of the fuel flow and jet engine RPM are on top of each other, and it is difficult to distinguish between the two, but that way we can see how the jet engine speed follows the change in the fuel flow and not the excitation voltage. This is the result of one of the runs. Let us take, for example, the time period between 50 and 100 seconds, when the fuel flow lever was not changed. Yet when we change the excitation between maximum and minimum, we see small to no changes in the jet engine's RPM. This is because the turbo-generator is driven by air pressure and lacks a shaft connection between the turbo-generator and the jet engine. The small fluctuations in the fuel flow rate seen here are caused by the pumping system that we have no control over. The lever itself was not changed. Now looking at the time period between 115 and 170 seconds, when the excitation voltage was constant, every change in the fuel flow lever position caused a noticeable change in the jet engine's RPM.

- 2) The change in the excitation voltage (excitation current or magnetic load around the rotor), usually leads to a relatively more gradual change in the turbo-generator RPM. The turbo-generator has a limit of 10k RPM, if it exceeds it the system will automatically shut off.

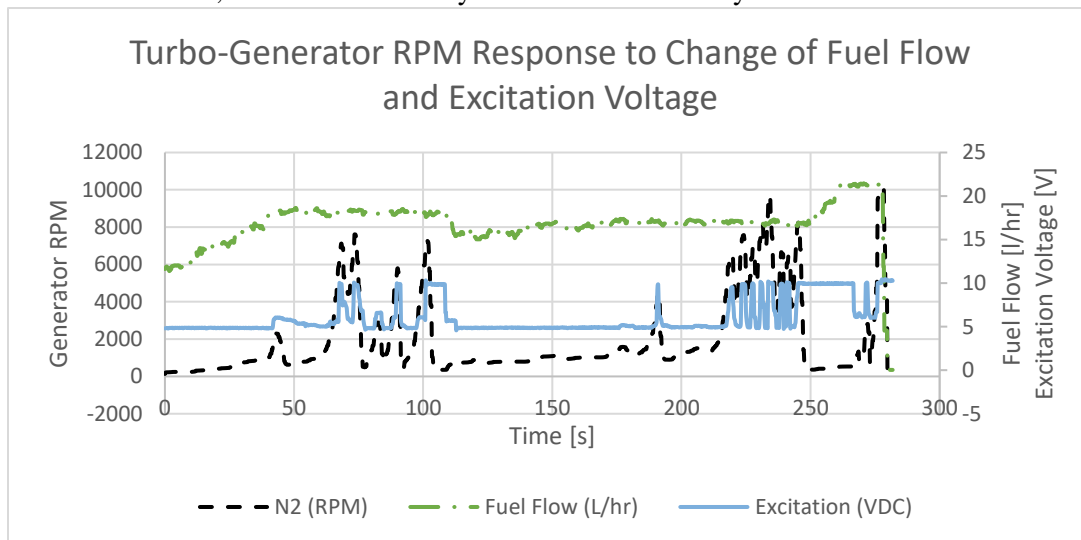


Figure 4.2: Turbo-generator RPM response to change in FF and excitation voltage. Black line (dashed line): turbo-generator RPM. Green line (dash-dotted): fuel flow rate. Blue line (solid line): excitation voltage. x-axis is in seconds.

This is the result from the same run as in Figure 4.1. Let us take for example the time period between 115 and 150 seconds, when the excitation voltage lever was not changed. Yet when we change the fuel-flow we see small to no changes in the turbo-generator's RPM. Now looking at the time period between 200 and 250 seconds, when the fuel flow lever was constant, every change in the excitation voltage lever position caused a noticeable change in the turbo-generator's RPM. The small fluctuations in the fuel flow rate seen here are caused by the pumping system that we have no control over. The fuel flow lever itself was not changed.

- 3) From the previous two points, the thermo dynamic connection and lack of shaft connection between the jet engine and turbo-generator (weak coupling between the jet engine and the turbo-generator) makes it so that change in excitation voltage affects the turbo-generator's RPM while it does not have an effect on the jet engine's RPM. Also, the fuel flow affects the jet engine's RPM far more than how it affects the turbo-generator's RPM.

- 4) There are 12 poles in the turbo-generator to create the 3-phase electricity for the load. We concluded this from the measurement of electrical frequency and rotational speed of the turbo-generator, as the author was not allowed to open the system for visual inspection.
- 5) The equation of conversion between turbo-generator's RPM and electric frequency is:

$$f = \frac{RPM_{generator}}{60 [\text{seconds in a minute}]} * \frac{12[\text{poles}]}{2} = \frac{RPM_{generator}}{10} [Hz] \quad (4.1)$$
- 6) The system in an open loop always has a stable jet engine RPM no matter what the inputs are, yet the turbo-generator RPM can only be stable while it rotates in the range of 150-1000 RPM (because the system's generator RPM sensor shows only values above 150 RPM). If the turbo-generator's RPM is greater than 1000 RPM with both inputs' constant, then it will keep accelerating until it becomes greater than 10000 RPM and activates the automatic shutdown. Even though the rotor accelerates, it still can be slowed down by increasing excitation voltage. One might think at first that the instability in the turbo-generator's RPM is due to lack of load, yet there is a load connected at all given times. The author investigated the reason for this instability and will be shown on in section 4.3 .
- 7) Phase resistance of the load side is: $R_{phase} = 0.12\Omega$. This load resistance is low, yet the maximum terminal voltage measured was 13.1 V. making the maximum output power equal to 1,430 W.
- 8) The author analyzed the internal piping of the system to start thinking of implementation for the fuel regulation. Although the fuel in this system is used for both the jet engine and cooling the turbo-generator, regulating the intake of the jet engine will not affect the cooling system.
- 9) The author analyzed the internal electric circuits in the system to start thinking of implementation for excitation regulation.

4.2 Steady-state analysis and constraints

The next step was analyzing the steady-state behavior of the system and the relation between the inputs and the outputs, as well as the Bristol gains. We received the system with software for measuring and logging data from the turbine, such as pressure, temperature, fuel flow rate, excitation voltage, generated voltage, frequencies, etc. The run procedure was as follows:

- a) Run the turbine in steady-state (turbo-generator RPM below 1000). Let it run for a while to have a good average for the steady-state supply voltage and turbo-generator RPM.
- b) Create a step change in one of the inputs and let the system get steady.
- c) Create a step-change in the second output and let the system get steady.
- d) Repeat steps "b" and "c" several times.

Conditions for the test:

- 1) Fuel flow between 11 l/h and 14 l/h. The system's limit is between 10 l/h and 20 l/h.
- 2) Excitation voltage range between 4.8 and 5V, where the lowest is 4.7V. The system's limit is between 4.7 V and 10 V.
- 3) Turbo-generator's RPM between 250 and 750 RPM. The manufacturer permits the system to operate between 150 RPM and 10000 RPM.

The reason we chose such small deviations in the inputs is due to the discoveries mentioned above (specifically point number 6 in section 4.1). We want to have steady data at a steady-state.

We define the system's Laplace transform matrices and vectors as:

- 1) Input: $\mathbf{U} = \begin{bmatrix} \text{fuel flow} \\ \text{excitation voltage} \end{bmatrix}$
- 2) Plant: $\mathbf{P} = \begin{bmatrix} K_{11} & K_{12} \\ K_{21} & K_{22} \end{bmatrix}$
- 3) Output: $\mathbf{Y} = \begin{bmatrix} \text{supply voltage} \\ \text{generator RPM} \end{bmatrix}$.

Although in this dissertation the output should be supply voltage and frequency, it has been shown in equation (4.1) that the conversion between turbo-generator RPM and frequency is quite simple. Therefore, the analysis can proceed in RPM as it is what the manufacturer provides as information in the software. Later on it can be converted with ease.

Usually while analyzing a generator there is a need to measure or specify stator resistance, synchronous impedance, open-circuit and short-circuit. Yet, the author did not measure or specify them as there was no information in the literature mentioning them. Also, there was not mention of the load and the author did not want to remove the load or short it, in order to keep the warranty on the system.

To have an initial understanding of the system and the interaction between the two loops as in the definition above, a calculation of the plant transfer function is needed. To calculate the plant transfer function ($K_{i,j}, i, j = 1, 2$), the author ran the system, kept it in a steady-state and each time changed one input and calculated the change on both outputs. These calculations are only good for steady-state operation and not for the whole system frequency response and cannot be used for stability calculation.

$$\begin{aligned} K_{11} &= \frac{\Delta(\text{supply voltage})}{\Delta(\text{fuel flow})} & K_{12} &= \frac{\Delta(\text{supply voltage})}{\Delta(\text{excitation voltage})} \\ K_{21} &= \frac{\Delta RPM}{\Delta(\text{fuel flow})} & K_{22} &= \frac{\Delta RPM}{\Delta(\text{excitation voltage})} \end{aligned} \quad (4.2)$$

By running multiple tests in an RPM range of 150 and 1000 and averaging the plant transfer function in steady-state, this method will give an initial indication as of how the system works. The dynamic model will be analyzed and explained later with consideration for uncertainty in the system. A steady-state results yield:

- 1) Plant: $\mathbf{P}(0) = \begin{bmatrix} 0.27 & -0.54 \\ 91 & -190 \end{bmatrix}$. It can be observed from the plant transfer function matrix, that as the excitation voltage increases the supplied voltage decreases. Supplied voltage is related to the rotational speed of the turbo-generator and the excitation voltage, meaning as the excitation voltage increases so should the supplied voltage. Yet, as it will be shown later in the analysis for the system, as the excitation voltage increases the rotational speed of the turbo-generator will significantly decrease, which is why the supplied voltage will decrease as excitation voltage increases. It is important to note that the system came with a fixed load and after the dynamic analysis the resistive load was changed without changing or adding reactance. Hence, an open-circuit and short-circuit experiment could not be conducted as the manufacturer did not include guidelines regarding impedance change.
- 2) To further understand how to change the two inputs in order to affect only one of the two outputs such as in considerate control, start by calculating the inverse of the plant matrix then calculate the determinant. The plant is in order:

$$\mathbf{P}^{-1} = \begin{bmatrix} 87.96 & -0.25 \\ 42.13 & -0.125 \end{bmatrix} \quad (4.3)$$

The determinant of inversed plant matrix yields:

$$\det(\mathbf{P}^{-1}) = \frac{1}{(87.96) \times (-0.125) - (42.13) \times (-0.25)} = -0.46 \quad (4.4)$$

Equation (4.4) shows that the determinant of the inverse matrix is close to being singular. For example, if we want to increase RPM only by 100 (10 electrical Hz) while keeping supply voltage constant, we will use the following equation to calculate the required change in the input:

$$\Delta \mathbf{U} = \mathbf{P}^{-1} \times \Delta \mathbf{Y} = \begin{bmatrix} 87.96 & -0.25 \\ 42.13 & -0.125 \end{bmatrix} \times \begin{bmatrix} 0 \\ 100 \end{bmatrix} = \begin{bmatrix} -25 \\ -12.5 \end{bmatrix}.$$

This small speed change requires simultaneous decreasing of fuel flow by 25 l/h and decreasing of excitation voltage by 12.5 V, which is physically impossible within the input ranges. The fuel flow range is 10 to 21 l/h, and the excitation voltage range is 4.7 to 10 V.

- 3) Bristol Gains array[24]: as seen in equation (3.15) both elements on the main diagonal will be equal. The rest of the elements will be calculated using the property that the sum of both elements must be one. By applying the number from the plant mentioned above we get the following result

$$\mathbf{B}(0) = \begin{bmatrix} 23.75 & -22.75 \\ -22.75 & 23.75 \end{bmatrix}. \quad (4.5)$$

These Bristol gains are too high, which means that a small deviation of one input would result in changes of both inputs that are out of the allowed range. There are other difficulties within two-loop control that are described later [9].

As a consequence, this turbine is unsuitable for the original goal of independent control of frequency and voltage. We suspect this problem comes from the extremely weak connection between the jet engine and turbo-generator. As mentioned above, while most electricity turbo-generators are connected to the jet engine through a shaft, the system that we have is connected thermodynamically via mass flow, meaning the only thing driving the rotor in the turbo-generator is the exhaust flow from the jet engine. Thus, as the turbine speed increases, the mass-flow of gas through the turbo-generator turbine increases. This transfers power from the fuel flow to the electrical output, yet with huge losses.

This connection has a downfall of low efficiency: it can be shown that the efficiency between the jet engine to electricity production is no more than 1.75% which can be achieved when the turbo-generator is pushed to the limit. In other words, high turbo-generator RPM cannot be controlled to be in steady-state without a stabilizing feedback.

The high Bristol gains is the reason why the initial research aim of 2×2 system cannot be pursued, as it is impossible to design 2 independent control loops because of the Bristol numbers, or in other words because of the large interaction.

4.3 Analysis of the system

In order to continue the research [25], another path was needed. The next step was to dig deeper, and not only have the basic analysis of the TurboGen. In other words, we wanted to understand the relationship between fuel flow, frequency, voltage, and other variables in the system. This was done in order to find the

plant's equations. This modelling would give us a better understanding of the system and it opens the path for designing the feedback control loop. This analysis was published [25] by the co-supervisor and the author.

4.3.1 Energy balance in turbogenerators

In order to understand the relationships between frequency, voltage, and other variables in and around a TurboGen unit, we begin with the fundamental law of energy conservation: the rate of energy change in a system is equal to the energy transfer rate across the system boundary. In general, energy may be transformed from other quantities within the system boundaries, but this is irrelevant for the present purposes.

The system of interest is the turbo-generator with a fixed load with two values. The turbo-generator is coupled on the common access. The turbo-generator is not connected to the jet engine by using a shaft and a gear box. If we ignore the changes in the internal energy of the turbo-generator, then the only relevant part is the rotational kinetic energy $J\Omega^2/2$. J is the effective rotational inertia of the turbo-generator and Ω is the angular speed of rotation. As already explained, because there are 12 poles the turbo-generator rotation speed is less than the angular frequency of the power supply (rad/sec).

The energy transfer rate is power. The turbine receives some of the fuel power P_{fuel} that is combusted (burned). This amount may be significantly less than the combustion power – especially when the primary role of the turbine is to generate mechanical thrust that is not used for electrical energy generation. The fraction of the fuel power that is coupled to the turbo-generator can be called the efficiency η . The turbo-generator delivers electrical power P_{el} . Thus, the energy balance equation can be written as:

$$\frac{d(J\Omega^2/2)}{dt} = P_{fuel}\eta - P_{el} \quad (4.6)$$

It is of interest that in steam-powered turbine-generator units[36], the fuel power is first converted into steam energy and the accumulated steam energy in the boiler needs to be modeled similarly to eq. (4.6).

In the case of a DC generator, the generated electrical power is simply the instantaneous product of voltage and current. We are considering the three-phase AC generators further. If U and I denote the root mean square (RMS) line voltage and line current respectively, then the three-phase generator delivers electrical power to a balanced three-phase load according to

$$P_{el} = \sqrt{3}UI \cos \phi \quad (4.7)$$

where $\cos \phi$ is the well-known power factor. ϕ is the phase angle between the sinusoidal phase-voltage and phase-current and it is equal to zero for ‘real’ or resistive loads. Much engineering effort is put into designing and operating electricity grids near unit power factor. The experimental turbo-generator is operated with a purely resistive load. Hence, $\cos \phi = 1$ is assumed in this dissertation without claiming that to be true for all turbo-generator operations.

4.3.2 A turbo-generator in island mode.

Now, we restrict attention to the case where a single turbo-generator unit supplies electrical energy to a balanced resistive three-phase load, just like in our case. In addition, we consider the load to be Y-

connected. If each phase resistance of the load is denoted with R_p then the supply line current is related to the electromagnetic force (between any two lines of a balanced system) as:

$$I = \frac{U}{\sqrt{3}R_p} \quad (4.8)$$

Therefore:

$$P_{el} = E^2/R_p \quad (4.9)$$

And:

$$\frac{d(J\Omega^2/2)}{dt} = P_{fuel}\eta - \frac{U^2}{R_p} \quad (4.10)$$

In steady-state, the turbo-generator rotates at a constant speed Ω and delivers electrical power at the line voltage.

$$U_{ss} = \sqrt{R_p P_{fuel}\eta} \quad (4.11)$$

The steady-state voltage does not depend on supply frequency (or turbo-generator speed Ω) – unless the turbine efficiency η depends on turbine speed and supply frequency. The supply voltage U must be controlled by varying the fuel flow rate (P_{fuel}). The calculation will be shown later in equation (4.23)

It may seem that the turbine speed – hence the supply frequency in a standalone operation of the turbo-generator – is not determined by the energy balance in eq. (4.10). However, inside the turbo-generator, the turbo-generator speed is related to the generated voltage through the magnetic field. Assuming negligible armature winding resistance, this relationship is approximated by:

$$E = k_1\Omega B \quad (4.12)$$

where B denotes the rotating magnetic field flux density in the air gap between the rotor and stator poles. Large turbo-generators have rotating electromagnets where the magnetic field is created and controlled by the excitation current I_x :

$$B = k_2 I_x \quad (4.13)$$

I_x is a DC current that may be connected to the rotor coils via slip rings, and it is normally much less than the supply current I . Equation (4.13) is a crude approximation only. In reality, the magnetic field may significantly saturate in a real rotor and there may be significant hysteresis too.

Power systems practitioners tell us that, despite the coils being inductors rotating in magnetic fields, the excitation current is proportional to the excitation voltage:

$$I_x = U_x/R_x \quad (4.14)$$

Usually in power systems equation (4.14) should include in the denominator also inductance or conductance[2], yet for this dissertation the author could not get information on the generator model. Nonetheless, the load connected to the generator outlet is pure resistance, which means that equation (4.14) is accurate enough for the model. With this understanding, equations (4.12) to (4.14) can be combined to

$$E = k_x\Omega U_x, \quad k_x = k_1 k_2/R_x \quad (4.15)$$

In a later section it will be shown how k_x and η are dependent on Ω . Also, the inductance in the equivalent circle of the generator could not be calculated, yet it is included in k_x .

However, eq. (4.10) does not allow constant rotor speed in case of transient power imbalances and, in steady-state, the excitation cannot affect the voltage in eq. (4.11). Instead, it controls the steady-state turbo-generator speed:

$$\Omega_{ss} = \frac{U_{ss}}{k_x U_x} = \frac{\sqrt{R_p P_{fuel} \eta}}{k_x U_x} \quad (4.16)$$

Eq. (4.10) can be rewritten as

$$\frac{d(J\Omega^2/2)}{dt} = P_{fuel}\eta - k_x^2 \frac{\Omega^2 U_x^2}{R_p} \quad (4.17)$$

with constant inertia,

$$\frac{d\Omega}{dt} = \frac{P_{fuel}\eta}{J\Omega} - k_x^2 \frac{\Omega U_x^2}{J R_p} \quad (4.18)$$

4.3.3 Experimental turbo generator in island mode

Our experimentation with the experimental turbo-generator has revealed a very strong efficiency dependence on turbo-generator speed – it improves dramatically as the turbo-generator speeds up. As a matter of fact, we are unable to maintain any steady-state above approximately 1000 RPM of the turbo-generator (corresponding to the supply frequency of 100 Hz). The jet engine speed is very stable, and it is not the problem. The turbo-generator turbine is stable at very low speeds when it is practically stalled. It ‘catches the wind’ only when it rotates fast enough and then it speeds up beyond the operational safety limit of 8000 RPM (not to be confused by the 10000 RPM limit that automatically shuts down the system as the manufacturer set).

Of the two manual control levers, the excitation voltage control seems more ‘immediately responsive’ in controlling the turbo-generator RPM. Hence, we tended to move the fuel flow control lever occasionally and leave it in positions corresponding to the (recommended) idle jet engine speed of 44000 RPM and up to about 65000 jet engine RPM. We then tried to manually stabilize turbo-generator speeds above 1000 RPM. It was impossible for us with the as-built electrical star-connected load of $R_p = 0.12 \Omega$ (Ohm) per phase. This load is created by a long metal as following:

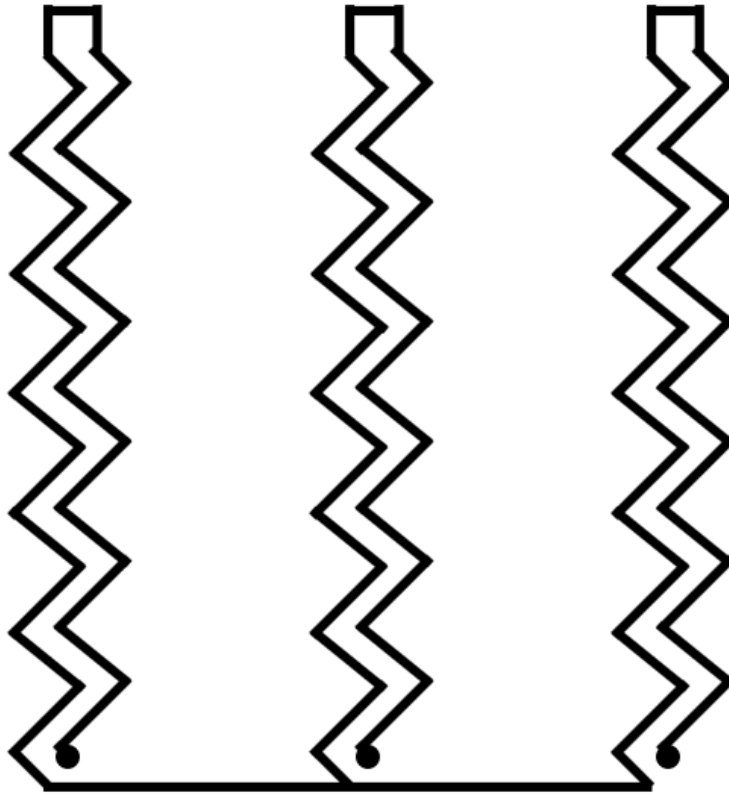


Figure 4.3: Y-connection of the three-phase resistor. Each resistor is 0.12Ω . The long horizontal line at the bottom is the neutral point.

To change the electrical load, a three-phase switch is connected to the three-phase load by having one end of each switch at the neutral point and the other end of the switches to the top of the resistor. That way when the switch is on the left side of each resistor it is short-circuited. The electrical load increases by halving the phase resistance to $R_p = 0.06 \Omega$ and we found it a little easier to handle turbo-generator speeds above 1000 RPM. The power balance will be shown later in figure 4.6 between inlet power and electrical power.

The following experiments were carried out with this increased load (decreasing R_p). In these experiments, we were able to leave both control levers in some (delicately tuned) fixed positions for turbo-generator speeds of up to about 1000 RPM. All data above 1000 RPM were obtained by intently observing (listening to) the turbo-generator speed and manually modifying the excitation lever. As the turbo-generator speed increased, it was harder to control it and keep it from accelerating, which meant moving the excitation lever to different positions in a fast manner. The turbo-generator speed fluctuated by a few 1000 RPM in a matter of seconds. This skill took many days to acquire, and it is not perfect. Attempts to keep the turbo-generator speed anywhere above 3000 RPM inevitably ended after a few tens of seconds with system shutdown due to turbo-generator speed reaching its design limit of 10000 RPM (again not to be confused with 8000 RPM which is the recommended upper safety limit for running the turbo-generator).

We have experimentally determined the following efficiency dependence on turbo-generator speed – see Figure 4.4. To calculate the efficiency, we solve eq. (4.6) for η :

$$\eta = \frac{P_{el} + d(J\Omega^2/2)/dt}{P_{fuel}} \quad (4.19)$$

As explained above, for turbo-generator speed between 0 and about 1000 RPM, the derivative term $d(J\Omega^2/2)/dt$ in eq. (4.19) is negligible and

$$\eta = \frac{P_{el}}{P_{fuel}}, \quad \Omega < 1000 \quad (4.20)$$

At first, equation (4.20) was used at all turbo-generator speeds to derive the efficiency data for Figure 4.4. The results were helpful but very ‘noisy’ at speeds above 2000 RPM. However, later we had to estimate the turbo-generator’s moment of inertia J anyway – we estimated it to be in the order of $0.003 \text{ kg}\cdot\text{m}^2$, as the company did not give us this information. This estimation was made as follows: by measuring the radius of the outer body of the turbo-generator, assuming that only half of it is the rotor, it yields a radius of 4.5 cm. The length of the rotor is assumed to be the length of the body, which is 5 cm. Lastly, the rotor is assumed to be made of steel with mass density of $8050 \text{ kg}/\text{m}^3$. Then, the inertia of a rotating cylinder central axis is $0.5R^2M = 0.003 \text{ kg}\cdot\text{m}^2$.

Then we recalculated the efficiency directly from equation (4.19). The smallest vertical spread was obtained with $J = 0.001 \text{ kg}\cdot\text{m}^2$. We take this to be a good estimate of the effective inertia. The results in the final edition of Figure 4.4 are obtained from equation (4.19) with $J = 0.001 \text{ kg}\cdot\text{m}^2$.

The following cubic function fits the data quite well up to 6500 RPM:

$$\eta(\Omega) = 6 \times 10^{-10} \left(\frac{\Omega}{1 \text{ RPM}} \right)^2 - 6 \times 10^{-14} \left(\frac{\Omega}{1 \text{ RPM}} \right)^3 \quad (4.21)$$

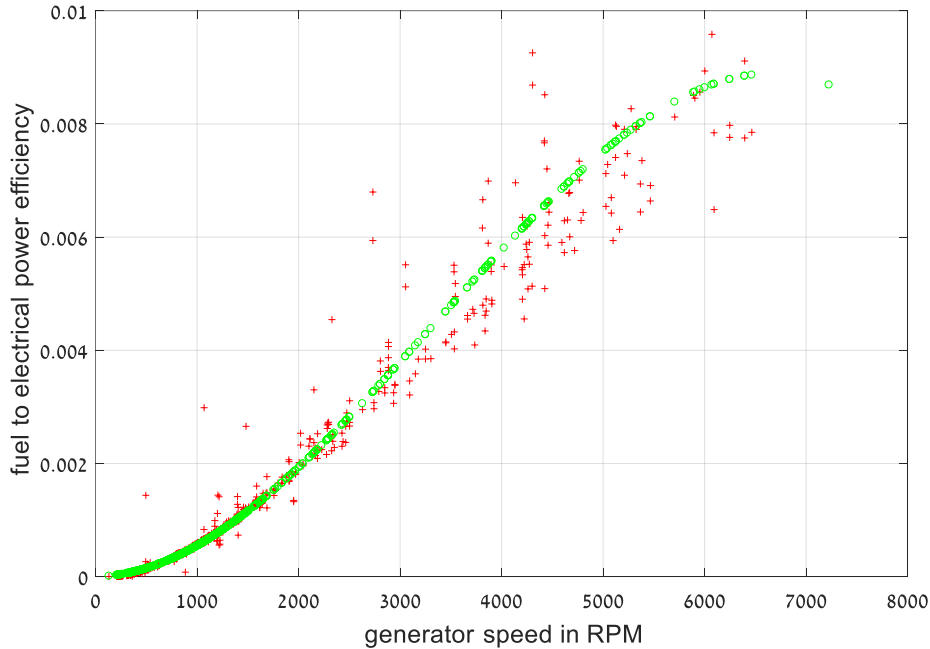


Figure 4.4: Turbine efficiency. The calculated experimental values of efficiency η are shown with red ‘+’. The cubic fit in eq. (4.21) is shown with green ‘o’.

It is important to understand the deceptively perfect fit of the cubic efficiency equations. It goes exactly to zero for zero speed. That tells us that the turbo-generator should not start up from zero speed – no fuel energy enters equation (4.6) and no electrical energy leaves the system at zero speed. Physically, efficiency cannot become exactly zero, because we always get the turbo-generator up and running with a sufficiently high fuel flow rate. We do not have enough information, nor any practical need, to include this extremely small speed effect in the model.

Figure 4.4 apparently indicates that the efficiency may saturate at around 0.8% or 0.9% above 6000 RPM. We do not completely trust this, because it is unreasonably low for an electrical energy turbo-generator in practice. While the veracity of this observation deserves to be investigated further, it is not of urgency for our purposes of operating the turbo-generator near 4000 RPM that, in our turbo-generator, corresponds to the ‘standard’ 400 Hz power supply in mobile applications.

Also, in figure 4.4 there are a lot of scattered points that clearly do not match the cubic function in equation (4.21), as they are far from the equation’s line and have a noticeable error. Yet, the scatter is caused due to the noise in the measurement system provided by the manufacturer. The author did design and implement another measurement circuit that will be discussed in chapter 5 with the addition of low-pass filter that enhances the quality of measurement, and in chapter 7 the behavior of the turbine in the closed loop system matches analysis done in this section also equation (4.21).

Usually, small scale systems have about 10% efficiency, yet this system cannot exceed 1% as provided by the manufacture[1], as well as from the results seen in figure 4.4. It is clearly an error in the design from the manufacturer, as the efficiency is quite low and not operable manually above 1000 RPM.

Next, we need to estimate the excitation coefficient k_x . To our surprise, it too varies significantly with the turbo-generator speed. We utilize the excitation equation $U = k_x \Omega U_x$. Here, every variable is measured, except the excitation coefficient. Hence, $k_x = U / (\Omega U_x)$. The calculated excitation coefficient’s dependence on turbo-generator speed is shown in Figure 4.5, where the trend is rather clear.

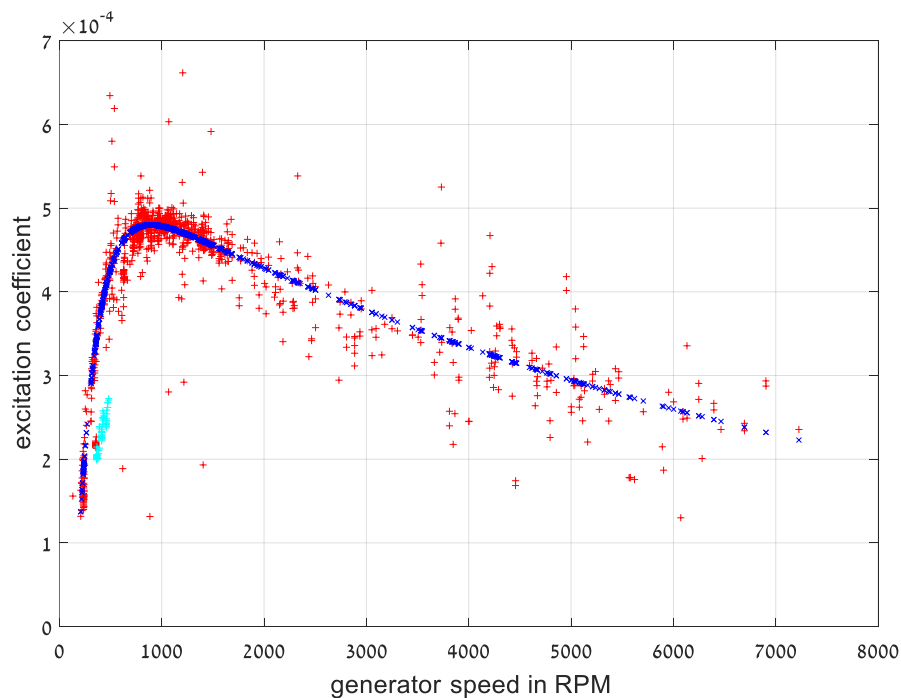


Figure 4.5: Excitation coefficient. The calculated experimental values of k_x are shown with red '+'. The exponential fit in eq. (4.22) is shown with blue 'x'.

The following exponential function – where the turbo-generator speed is measured in RPM – fits the data well up to 7500 RPM:

$$k_x(\Omega) = 5.5 \times 10^{-4} e^{-\Omega/8000} (1 - e^{-(\Omega-150)/200}) \sigma(\Omega - 150) \quad (4.22)$$

Most measurements were carried out near 5 V of excitation. The low-speed group of results, indicated in cyan, was obtained from measurements with a nearly maximum excitation voltage of 10 V. We are not entirely certain what causes the low-frequency decline of the excitation coefficient, but we suspect magnetic saturation there. At higher speeds, we suspect increasing slip ring-brush contact resistance. The drop in k_x is the effect of the equivalent inductance in series with the resistive load, as the voltage generated by the turbo-generator is divided on the reactance $j\omega L$ and resistance R_{load} . The increment in the range of 150 RPM and 950 RPM could not be investigated.

Also, in figure 4.5 there are a lot of scattered points that clearly do not match the cubic function in in equation (4.22), as they are far from the equation's line and have a noticeable error. Yet, the scatter is caused due to the noise in the measurement system provided by the manufacturer. The author did design and implement another measurement circuit that will be discussed in chapter 5 with the addition of low-pass filter that enhances the quality of measurement, and in chapter 7 the behavior of the turbine in the closed loop system matches analysis done in this section also equation (4.22).

Now we have all the relevant data to consider the energy conservation equation (4.17) further. In any steady state, there must be a balance between the energy inflow rate $P_{in} = P_{fuel}\eta(\Omega)$ and energy outflow rate $P_{el} = k_x^2(\Omega)\Omega^2 U_x^2/R_p$. When $P_{in} > P_{el}$, then the turbo-generator accelerates, and when $P_{in} < P_{el}$, then the turbo-generator decelerates. This helps to understand stability.

The minimum fuel flow rate to reach the recommended jet engine idle speed of 44000 RPM is about 13 liters per hour. We typically use a measured fuel flow rate of around 17 liters per hour giving us a jet engine speed of around 58000 or 59000 RPM. The calorific value of the A1 fuel is 35 MW/liter. Hence, we typically have $P_{fuel} = 165\text{kW}$. The excitation voltage is variable only between 5 and 10 Volts.

The turbo-generator speed, efficiency, and excitation coefficient need to be expressed in SI units. Since 1 RPM=0.1 Hz, equations (4.21) and (4.22) become:

$$\eta(\Omega) = 6 \times 10^{-8} \Omega^2 - 6 \times 10^{-11} \Omega^3 \quad (4.23)$$

$$k_x(\Omega) = 5.5 \times 10^{-3} e^{-\Omega/800} (1 - e^{-(\Omega-15)/20}) \sigma(\Omega - 15) \quad (4.24)$$

Here, Ω is measured in rad/s. The two energy flow rates are compared graphically in Figure 4.6 for a fuel flow rate of 17 liters per hour and excitation voltages at 5.7V. With these constant inputs, there are two, or maybe three steady-state speeds.

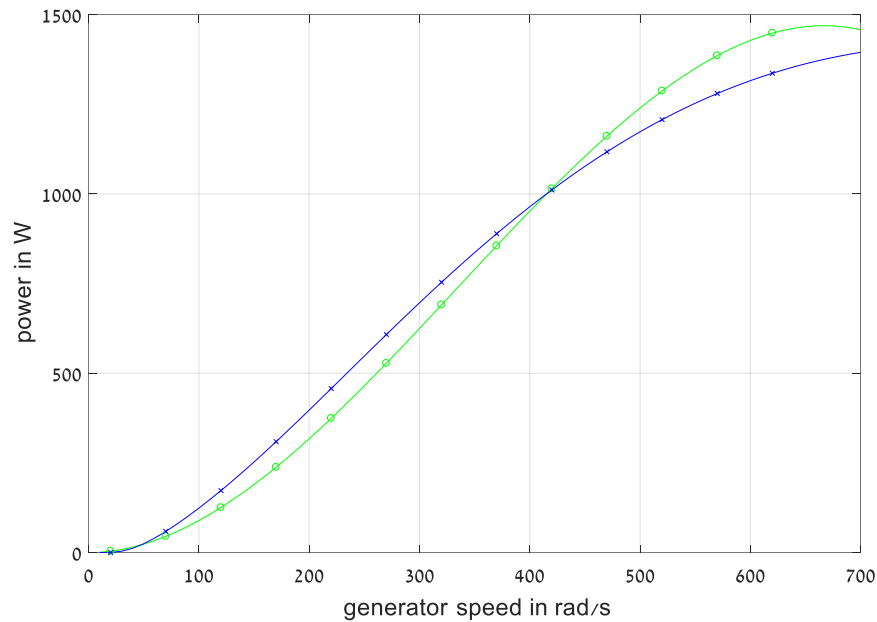


Figure 4.6: Energy flow balance. P_{in} is shown with green ‘o’. P_{el} is shown with blue ‘x’. Fuel flow of 17 liters per hour and $U_x = 5.7V$.

In figure 4.6, $P_{in} = P_{fuel}\eta(\Omega)$ and $P_{el} = k_x^2(\Omega) \Omega^2 U_x^2 / R_p$. There is one steady turbo-generator speed at very low value of 47 rad/s – see also the zoomed view in Figure 4.7. This is a *stable* point, because a speed below 47 rad/s causes the turbo-generator to accelerate and a speed above 47 rad/s causes the turbo-generator to decelerate.

There is another steady turbo-generator speed at 420 rad/s. This is an *unstable* point, because a speed below 420 rad/s causes the turbo-generator to decelerate and a speed above 420 rad/s causes the turbo-generator to accelerate. While there may be a third steady-state at much higher speeds – we have not been able to reach the third point.

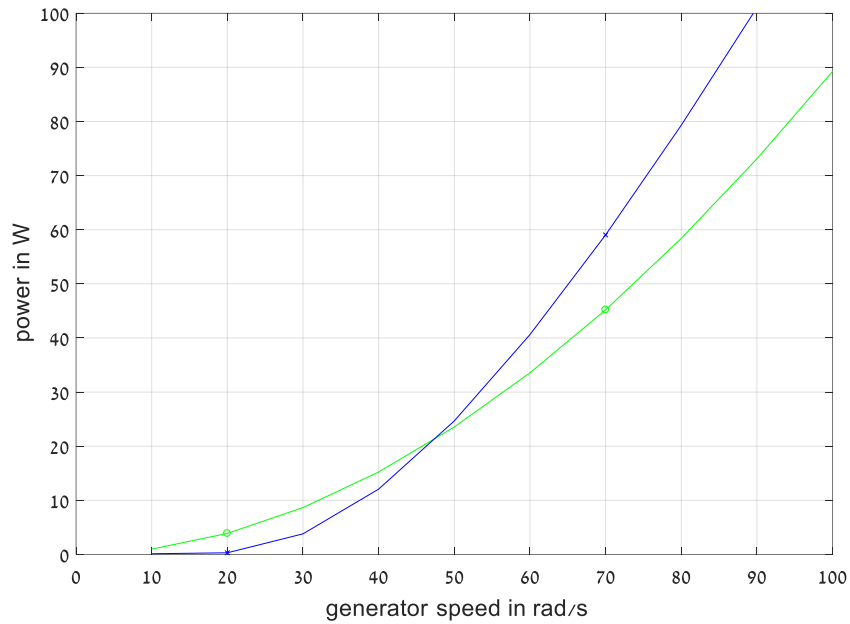


Figure 4.7: Energy flow balance. Zoomed in to stable operating point at about 47 rad/s.

The highest possible steady-state operating speed is about 100 rad/s. To reach this speed, one has to lower the excitation voltage or increase the fuel flow rate – relative to the values in Figure 4.5. Reducing the excitation to its minimum of 5 V is not sufficient. When, in addition, the fuel flow rate is increased to 18.3 liters per hour, then we get a marginally stable steady-state at about 100 rad/s in Figure 4.8.

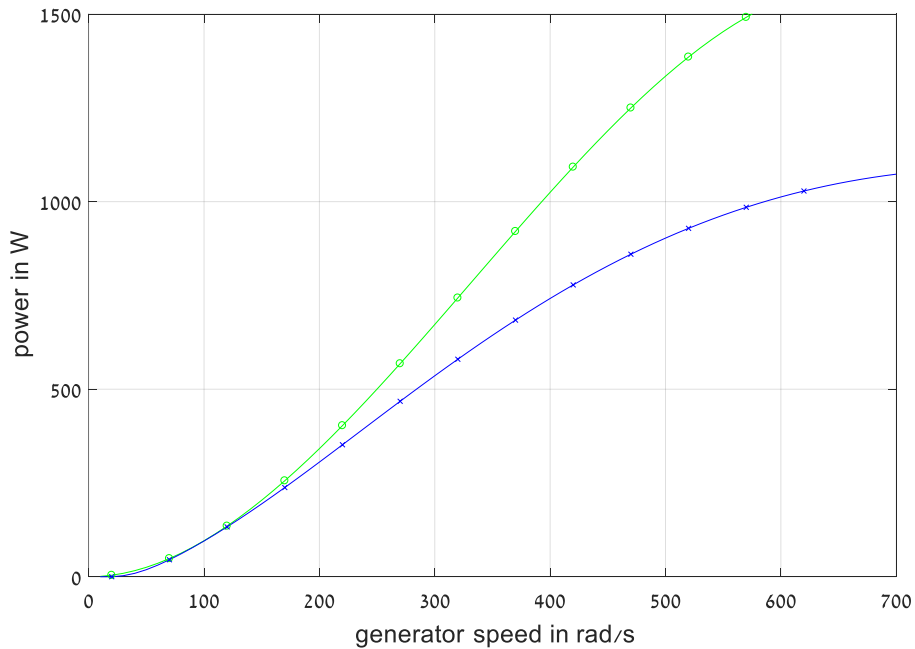


Figure 4.8: Energy flow balance. Pin is shown with green 'o'. Pel is shown with blue 'x'. Fuel flow of 18.3 liters per hour and $U_x = 5.0$ V.

If the fuel flow rate is increased just a little further, then the system does not have a steady state. The turbo-generator accelerates beyond 8000 RPM and is shut down at 10000 RPM.

4.3.4 Linearized model for experimental turbo-generator

Substitute $\eta = \eta(\Omega)$ from equation (4.23) and $k_x = k_x(\Omega)$ from equation (4.24) into equation (4.18):

$$\frac{d\Omega}{dt} = \left[P_{\text{fuel}}(6 \times 10^{-8} - 6 \times 10^{-11}\Omega) - k_x^2 \frac{U_x^2}{R_p} \right] \frac{\Omega}{J} \quad (4.25)$$

where $k_x = 5.5 \times 10^{-3} e^{-\Omega/800} (1 - e^{-(\Omega-15)/20}) \sigma(\Omega - 15)$

Let us find the linear model parameters for the above three steady-state conditions, at 47, 100, and 420 rad/s. They are expected to be stable, marginally stable and unstable respectively, as the system behaves accordingly. Because, when the Turbo-Gen's speed is below 1000RPM (100 rad/s) it remains is stable, while exceeding 1000RPM it becomes unstable, leaving the marginally stable point at 1000RPM.

For small deviations from any steady-state operating condition, we obtain from eq. (4.25)

$$\begin{aligned} \frac{d\Delta\Omega}{dt} = & - \left[P_{\text{fuel}}(6 \times 10^{-11}) + 2k_x \frac{U_x^2}{R_p} \frac{dk_x}{d\Omega} \right] \frac{\Omega}{J} \Delta\Omega + \\ & + [(6 \times 10^{-8} - 6 \times 10^{-11}\Omega)] \frac{\Omega}{J} \Delta P_{\text{fuel}} - \left[2 \frac{k_x^2 U_x}{R_p} \right] \frac{\Omega}{J} \Delta U_x \end{aligned} \quad (4.26)$$

The voltage equation (4.14) is similarly linearized to:

$$\Delta U = \left[k_x U_x + \Omega U_x \frac{dk_x}{d\Omega} \right] \Delta\Omega + [k_x \Omega] \Delta U_x \quad (4.27)$$

In both equations, we need the derivative:

$$\frac{dk_x(\Omega)}{d\Omega} = 5.5 \times 10^{-3} \left[\frac{-1}{800} e^{-\Omega/800} (1 - e^{-(\Omega-15)/20}) + e^{-\Omega/800} \frac{1}{20} e^{-(\Omega-15)/20} \right] \quad (4.28)$$

Introducing the coefficients:

$$\begin{aligned} a &= \left[P_{\text{fuel}}(6 \times 10^{-11}) + 2k_x \frac{U_x^2}{R_p} \frac{dk_x}{d\Omega} \right] \frac{\Omega}{J} \\ b_{\text{fuel}} &= [(6 \times 10^{-8} - 6 \times 10^{-11}\Omega)] \frac{\Omega}{J} \\ b_x &= \left[2 \frac{k_x^2 U_x}{R_p} \right] \frac{\Omega}{J}; \quad c = \left[k_x U_x + \Omega U_x \frac{dk_x}{d\Omega} \right]; \quad d_x = [k_x \Omega] \end{aligned} \quad (4.29)$$

allows the above state equations to be written in the more compact form below:

$$\frac{d\Delta\Omega}{dt} = -a\Delta\Omega + b_{\text{fuel}}\Delta P_{\text{fuel}} - b_x\Delta U_x \quad (4.30)$$

$$\Delta U = c\Delta\Omega + d_x\Delta U_x \quad (4.31)$$

The following table summarizes the three sets of parameter values.

Ω	P_{fuel}	U_x	a	b_{fuel}	b_x	c	d_x
[rad/s]	[kW]	[V]	[rad /s]	[rad /(s^2W)]	[rad /(s^2V)]	[Vs]	
47	165	5.7	$0.0104/J$	$2.69e^{-6}/J$	$0.153/J$	0.0362	0.194
100	178	5.0	$6e-5/J \approx 0$	$5.40e^{-6}/J$	$0.382/J$	0.0227	0.478
420	165	5.7	$-0.0019/J$	$1.46e^{-5}/J$	$0.845/J$	0.0088	1.367

Table 4.1: Three sets of linearized state equation parameters with measured $R_p = 0.06 \Omega$. $J \approx 0.001 \text{ kg} \times m^2$.

The output and input variables are combined in the output and input vectors:

$$\mathbf{Y} = \begin{bmatrix} Y_1 \\ Y_2 \end{bmatrix} = \begin{bmatrix} \Delta \text{voltage} \\ \Delta \text{speed} \end{bmatrix}; \quad \mathbf{U} = \begin{bmatrix} U_1 \\ U_2 \end{bmatrix} = \begin{bmatrix} \Delta \text{fuel} \\ \Delta \text{excitation} \end{bmatrix} \quad (4.32)$$

$$\mathbf{Y} = \mathbf{P}\mathbf{U} \quad (4.33)$$

Applying the Laplace transform to the equations (4.30) and (4.31) yields the four transfer relationships in the transfer matrix \mathbf{P} :

$$\mathbf{P}(s) = \begin{bmatrix} \frac{b_{fuel}c}{s+a} & \left(d_x - \frac{b_x c}{s+a} \right) \\ \frac{b_{fuel}}{s+a} & -\frac{b_x}{s+a} \end{bmatrix} = \begin{bmatrix} \frac{b_{fuel}c}{s+a} & \frac{d_x s + (ad_x - cb_x)}{s+a} \\ \frac{b_{fuel}}{s+a} & -\frac{b_x}{s+a} \end{bmatrix} \quad (4.34)$$

Substituting numbers from Table 4.1 yields the following three transfer matrices, indicated by the relevant steady-state turbo-generator speeds.

$$\mathbf{P}_{47}(s) = \begin{bmatrix} \frac{9.74 \times 10^{-5}}{s+10} & \frac{0.194s - 3.5}{s+10} \\ \frac{2.69 \times 10^{-3}}{s+10} & \frac{-153}{s+10} \end{bmatrix} \quad (4.35)$$

$$\mathbf{P}_{100}(s) = \begin{bmatrix} \frac{1.22 \times 10^{-4}}{s} & \frac{0.478s - 8.6}{s} \\ \frac{5.40 \times 10^{-3}}{s} & \frac{-382}{s} \end{bmatrix} \quad (4.36)$$

$$\mathbf{P}_{420}(s) = \begin{bmatrix} \frac{1.29 \times 10^{-4}}{s-2} & \frac{1.37s - 100}{s-2} \\ \frac{1.46 \times 10^{-2}}{s-2} & \frac{-845}{s-2} \end{bmatrix} \quad (4.37)$$

Note that – not unexpectedly – the excitation to supply voltage transfer in P_{12} is not strictly proper in the crude model as seen in equation (4.34). In reality, there will be some electrical lag. It is assumed here that the mechanical turbine inertia is significantly greater than the electrical inertia in the excitation sub-system.

Previously in this section, the steady-state gains of the plant transfer function in equation (4.2) were calculated from experimental results. Now comparing to the plant transfer function in equation (4.34) in steady-state ($s \rightarrow 0$), first the parameters are calculated with the following results:

Ω	P_{fuel}	U_x	a	b_{fuel}	b_x	c	d_x
[rad/s]	[kW]	[V]	[rad /s]	[rad /(s^2W)]	[rad /(s^2V)]	[Vs]	
34.6	155	10	19.16	0.002	65.4	0.067	0.119
38.6	192	10	19.05	0.002	88.9	0.067	0.147
45.9	155	8	10.981	0.002	107	0.052	0.196
56	165	7.5	7.317	0.003	146	0.045	0.262
60.7	165	7.3	5.848	0.003	162	0.042	0.291
67.9	175	7.3	4.324	0.003	190	0.04	0.334
81.3	185	7.3	2.044	0.004	237	0.036	0.407
87.1	186	7.3	1.296	0.004	255	0.035	0.437
92	194	7.43	0.791	0.005	274	0.035	0.462

Table 4.2: Three sets of linearized state equation parameters with measured $R_p = 0.12 \Omega$.

which results in the steady-state plane matrix of:

$$\mathbf{P}(s \rightarrow 0) = \begin{bmatrix} 62 * 10^{-6} & -2.858 \\ 1.7 * 10^{-3} & -85.54 \end{bmatrix} \quad (4.38)$$

Keep in mind that the linearized model is meant for small deviations around a steady-state point. The larger the deviation, the less accurate the model becomes. Now, converting the plant transfer function in steady-state from the initial experimental results in equation (4.2), while converting from $\Delta(\text{fuel flow})$ to $\Delta(P_{fuel})$ by multiplying the left column by $3600/35 * 10^6$, which is the conversion from l/h to J/s, yields:

$$\mathbf{P}(s \rightarrow 0) = \begin{bmatrix} 27 * 10^{-6} & -0.54 \\ 9.4 * 10^{-3} & -190 \end{bmatrix} \quad (4.39)$$

Although the left column in the plant transfer function from the experimental results in equation (4.2) is changed, yet the Bristol gains will bear no change and still be equal to the same as in the equation (4.5) matrix, where the main diagonal elements are equal to 23.75 and the secondary diagonal elements are equal to -22.75 . As for the linearized model, the Bristol gains from the equation (4.38) yields the following maximum and minimum Bristol gains:

$$\mathbf{B}_{min}(s \rightarrow 0) = \begin{bmatrix} 1.92 & -0.92 \\ -0.92 & 1.92 \end{bmatrix} \quad (4.40)$$

$$\mathbf{B}_{max}(s \rightarrow 0) = \begin{bmatrix} 26.34 & -25.34 \\ -25.34 & 26.34 \end{bmatrix} \quad (4.41)$$

Comparing between the Bristol gains from the linearized model in equations (4.40) and (4.41) and the Bristol gains from the steady-state experiments in equation (4.5), it can be seen that the Bristol gains in equation (4.5) that is equal to 23.75 is within the range between given in equations (4.40) and (4.41) which is between 1.92 and 26.34. Although the experimental Bristol numbers are closer to the upper limit from the Bristol gains in the linearized model, it is caused by the averaging of the results done in the experiment. Meaning that the theoretical linear model and the experiments do match.

The formal system block diagram is given in Figure 4.9. It serves the purposes of interaction analysis and quantitative feedback design well. On the other hand, it hides the fact that the four transfer functions are generally not independent, and their states are not separate.

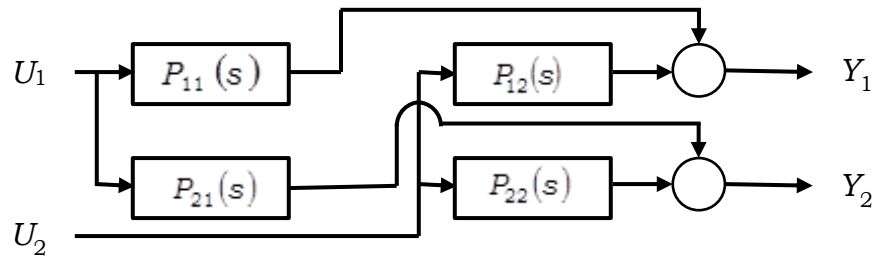


Figure 4.9: Formal linear turbo-generator block diagram.

For many purposes, a better understanding is obtained from the physically motivated block diagram in Figure 4.10.

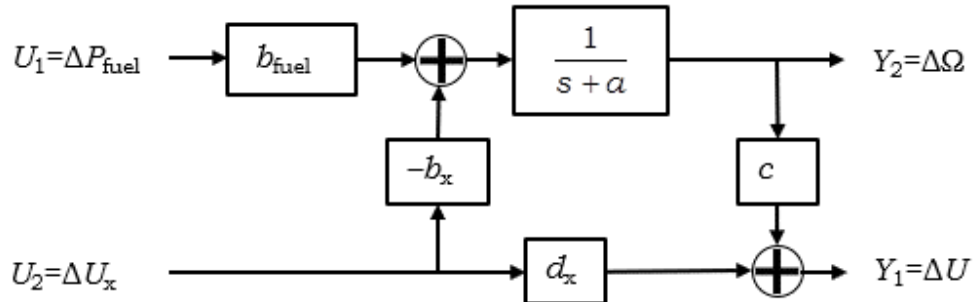


Figure 4.10: Physically motivated linear turbo-generator block diagram.

In Figure 4.10, the low frequency gain (from U_2 to Y_2) is $d_x - \frac{b_x c}{a} = 0$ – in the ideal case of constant efficiency. This gain is significantly non-zero in our far from ideal turbo-generator.

4.3.5 Choice of input output pairing for experimental turbo-generator

The system transfer matrix from equation (4.34) can be written as:

$$\mathbf{P}_\Omega(s) = \begin{bmatrix} p_{11\Omega} & sp_{12\Omega} \\ p_{21\Omega} & p_{22\Omega} \end{bmatrix} \frac{1}{s + a_\Omega} \quad (4.42)$$

Hence, the Bristol gain simplifies to

$$B_{\Omega}(s) = \frac{p_{11\Omega}p_{22\Omega}}{p_{11\Omega}p_{22\Omega} - p_{21\Omega}p_{12\Omega}(s)} \quad (4.43)$$

From equations (4.35) to (4.37) we obtain the following Bristol gains.

$$B_{47}(s) = \frac{2.7}{1 + \frac{s}{10}} = \frac{2.7}{1 + \frac{s}{a_{47}}} \quad (4.44)$$

$$B_{100}(s) = \frac{18}{s}, \quad \{a_{100} = 0\} \quad (4.45)$$

$$B_{420}(s) = \frac{-2.9}{1 - \frac{s}{1.9}} = \frac{-2.9}{1 + \frac{s}{a_{420}}} \quad (4.46)$$

Clearly in low frequency (lf) (for $s \rightarrow 0$), $|B_{lf}| \gg 1$ and in high frequency (hf) (for $s \rightarrow \infty$), $B_{hf} = 0$. Note that here we are referring to the ‘control frequency’ ω – the imaginary part of the Laplace variable s . It is of interest to note that when the $P_{in}(\Omega)$ and $P_{el}(\Omega)$ curves are parallel then $B_{lf} \rightarrow \infty$.

In the frequency range of interest, the low frequency Bristol gain magnitude is theoretically no less than 3. A few experimental evaluations of the steady-state Bristol gain has indicated in similar testing conditions that the Bristol gain magnitude is actually about 8 and greater. Within the narrow input limitations available to us, we have to abandon independent control of the supply voltage and frequency.

4.4 Conclusions

A high efficiency turbo-generator in island mode (in stand-alone operation) is inherently stable, and it allows independent control of supply voltage and frequency. Our experimental turbo-generator, however, behaves very differently. It is unstable over most of the turbo-generator operating frequency range and its voltage and frequency cannot be controlled independently.

Also, the plant in equation (4.42) has a pole at $-a$. The value of a can be:

- 1) $a > 0$: this means that the pole is in the LHP, and the system is stable. It happens when the turbo-generator’s speed is under 1000 RPM.
- 2) $a = 0$: this means that the pole is at the origin. This happens when the turbo-generator’s speed is approximately 1000 RPM.
- 3) $a < 0$: this means that the pole is in the RHP making the system unstable. This happens when the turbo-generator’s speed is greater than 1000 RPM.

It seems is that the instability is caused by the increase in efficiency with speed being dominant over the increase in internal voltage with speed. The effect is that the additional power is not sent out to the electrical load and hence accelerates the machine because the turbo-generator has low moment of inertia, and the power imbalances result in fast dynamics.

Chapter 5

Theoretical Design

In the previous chapter, it was shown that the experimental turbo-generator used for this dissertation is unstable once the generator's RPM goes over 1000. Also, because of the strong interaction between the two loops, this system cannot have a 2×2 control system with the given inputs' range of excitation voltage and fuel flow. A modified specific goal is formulated as follows: in section 4.3.2 it was shown that for the generator used in the dissertation, the steady-state supply voltage should be controlled through fuel flow, and the supply frequency through the excitation voltage, which is the opposite of what is used as input-output pairs in an electricity generation in a grid [2].

Thus, a new aim is set: design a digital feedback control system that regulates the supply frequency (output) around 400 Hz, by feeding it back to the excitation voltage (input).

In this chapter, all the transfer function frequency responses will be shown upon a sensitivity chart (S-Chart)[14], which is the inverse of the Nichols chart (as the late professor Horowitz called it). In a Nichols chart the complementary sensitivity is shown as lines using the function $1/(1 + 1/L)$, whereas in the S-chart, the sensitivity lines are a function of $1/(1 + L)$.

5.1 Controller design

As mentioned above, we will be controlling the frequency (output) by regulating the excitation voltage (input). Also, in this project, the controller will be a digitally implemented PI controller and not analog PI. First step we need to display the frequency response of the system on the S-Chart, using the system's model mentioned in equation (4.37).

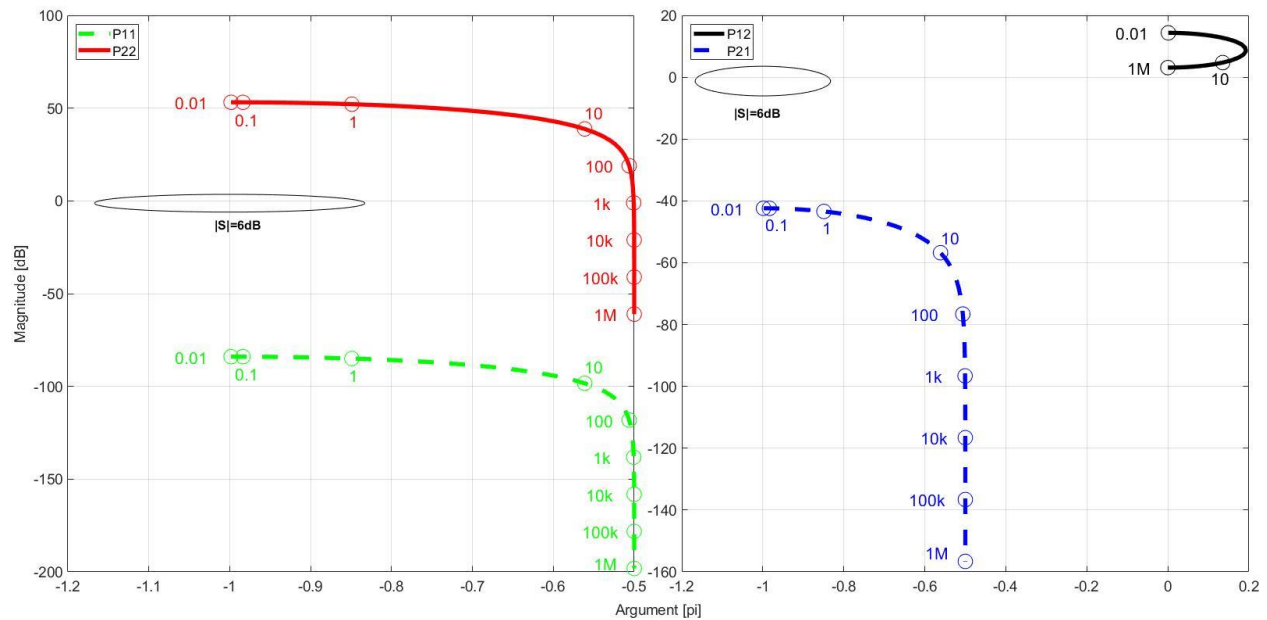


Figure 5.1: the system's frequency response at generator's RPM equal to 4200 with an added proportional controller of -1. Left graph P_{11} , dashed green line: fuel flow to supply voltage. Left graph P_{22} , solid red line: excitation voltage to generator RPM. Right graph P_{21} , dashed blue line: fuel flow to generator RPM. Right graph P_{12} , solid black line: excitation voltage to supply voltage.

In Figure 5.1, the plant transfer functions of P_{22} , P_{21} and P_{11} have a high-frequency response with a constant $Arg = -0.5\pi$. Also as the frequency gets greater, the magnitude of the transfer function gets smaller. This kind of behavior is most probably not that accurate of a model in the high-frequency range as it could not be measured. In reality, it should have more phase lag, thus leaving the high-frequency tuning to the controller implementation part.

Also, in figure 5.1, actually $-P_{22}(j\omega)$ is displayed. As $P_{22}(j\omega)$ at the operating point of 4200 generator RPM has a RHP pole in it, as explained in the previous section, meaning that at this operating point the system is unstable. By adding a proportional controller with a gain of -1 already, the closed-loop system will encircle the Nyquist point and stabilize the system. It can also be seen that the system is stable by going back to figure 4.10 by closing the loop by controller between the output of rotational speed $\Delta\Omega$ and input of excitation voltage ΔU_x . The closed-loop transfer function in figure 5.2 between the mentioned input-output pair would result in:

$$\begin{aligned} \Delta Y_{2U_2} &= R \frac{1}{1 + G(s) \frac{-b_x}{s+a}} \Bigg|_{G(s)=-1} = R \frac{1}{1 + \frac{b_x}{s+a}} = \\ &= R \frac{s+a}{s+a+b_x} \Bigg|_{a=-2; b=845} = R \frac{s-2}{s+843} \end{aligned} \quad (5.1)$$

meaning the RHP that existed in the transfer function in equation (5.1) would shift to the left half plane after closing the system and stabilizing it. Then the system will be as following:

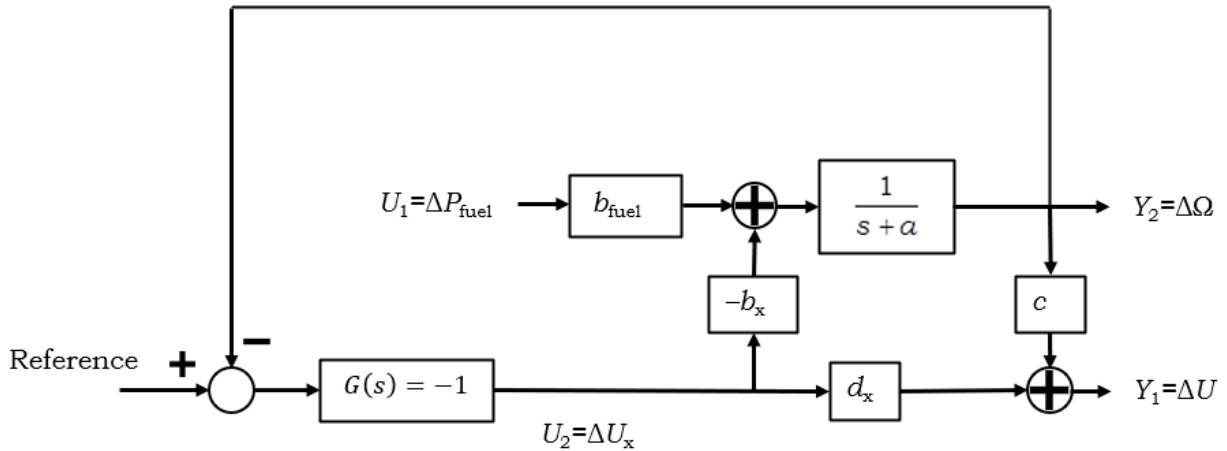


Figure 5.2: multivariable system with feedback loop and control.

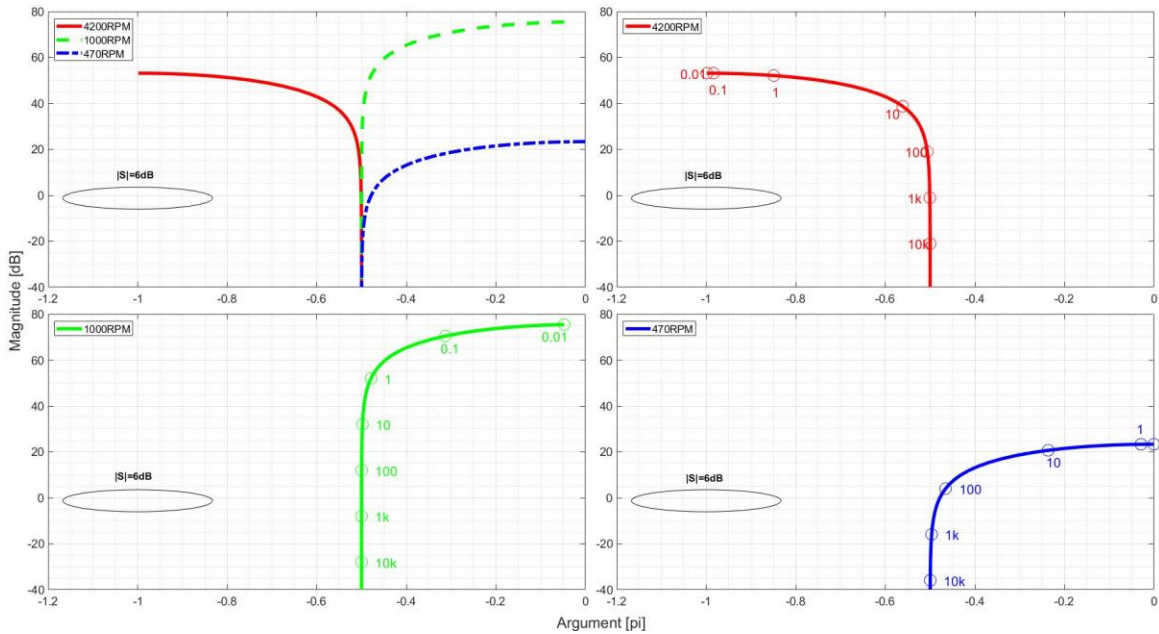


Figure 5.3: Top left graph, the loop, $L(j\omega) = kP_{22}(j\omega)$, frequency response at three operational points 47 Hz, 100 Hz, and 420 Hz. Here a proportional gain of $-1 \frac{V}{Hz}$ is used. Top right graph, frequency response at operational point 420 Hz. Bottom left graph, frequency response at operational point 100Hz. Bottom right graph, frequency response at operational point 47 Hz.

Figure 5.3 displays the three operating points of 42 Hz, 100 Hz and 420 Hz of the generator. Whereas the 42 Hz has a LHP pole, the 100 Hz is supposed to have a pole on the imaginary axes, or at least close to it, and as the RPM gets higher, the pole will shift from the LHP to the RHP as seen at 470 Hz. In a closed loop, without adding negative gain, the system will be unstable. By multiplying the loop with a -1 we will get a stabilizing encirclement of the Nyquist point in case of the unstable open-loop plant.

As mentioned by Eitleberg[4], to achieve a proper implementation of a digital controller, the guidelines are to start with the design in the analog world, meaning without the consideration of the sampling effect. After the design is complete, then we proceed into adding the sampling effect of $1 - wT/2$. By doing that we can figure out what is the lowest sampling speed available for the controller. However, with the micro-controller in use, the function for frequency measurement is predefined, as the function measures the elapsed time during a single cycle. Under this restriction, the sampling rate is already given per frequency, which also means that different working points give different sampling effects. Thus, the final step of the guideline must be used prior to designing the analog controller.

The predefined frequency measurement function in the micro-controller gives the result of the frequency after each elapsed time cycle, yet it is recommended by the manufacturer[35] of the micro-controller to average out multiple cycles for better accuracy. The author used a measurement of 6 cycles and then average the results to lessen the measurement error. Also, in the digital implementation paper [4] it is recommended to use an anti-aliasing filter in the input of the micro-controller. It was implemented not for the purpose of anti-aliasing, as the system is limited by frequencies of 0 Hz to 1 kHz, but as a low-pass filter. A low-pass filter is used for the anti-aliasing to eliminate the noises created by all the transformers and high voltage interactions. A first-order low-pass filter (LPF) with a corner frequency of 1 kHz sufficed, as the noises received by the controller are spikes that happen once in a while, meaning that they are high-frequency

noises approximately equal to 90 kHz. However, those spikes would contaminate the data, which may lead to incorrect calculations for the controller output.

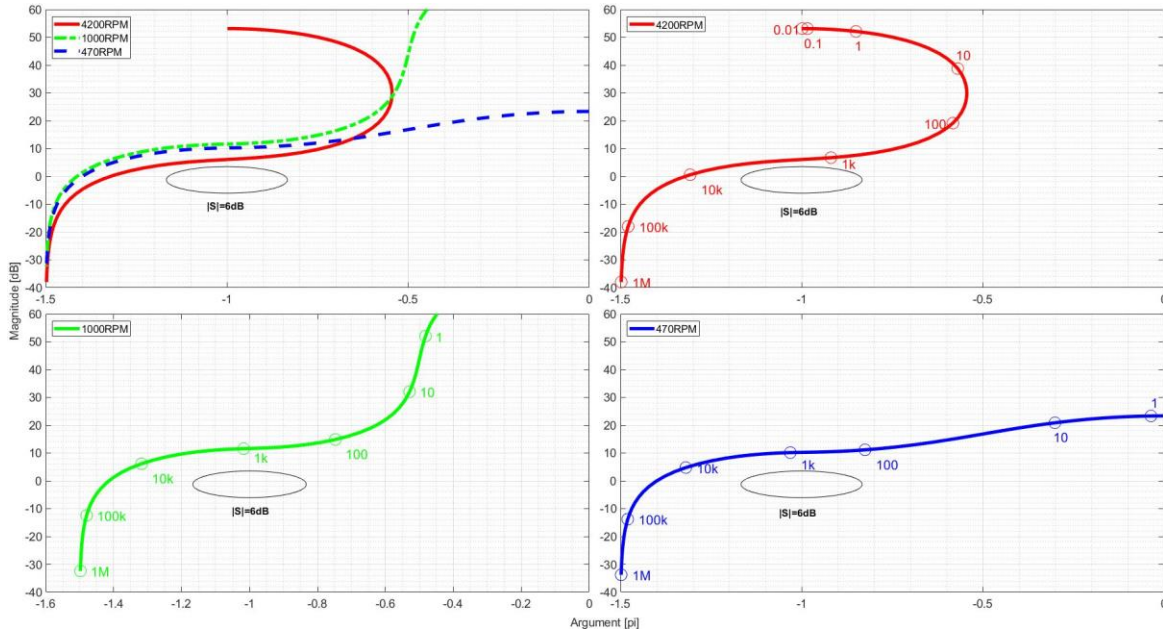


Figure 5.4: frequency response for P22 transfer function with the addition of sampling effect and first-order LPF. Top left graph combines all the operational points, red solid line for 4200 RPM, green dash dotted line for 1000 RPM and blue dashed line for 470 RPM. Top right graph, red line: P22 at the operating point of 4200 RPM. Left bottom: graph: P22 at the operating point of 1000 RPM. Right bottom graph: P22 at the operating point of 470 RPM.

In figure 5.4 compared to figure 5.3, adding the effect of the digital implementation affected the high frequency more than the low frequencies. Also as mentioned above, the sampling rate is equal to the electric frequency 6 samples, each sample is one cycle. This means that the digital implementation affects each operating point differently. To simplify matters, let us assume that the system is in steady-state, which means the supply frequency is constant. If for example the frequency is 420 Hz, 100 Hz and 47 Hz, then with the sampling time which is equal to 6 cycles leads to a 0.014 s, 0.06 s and 0.127 s sampling period respectively. Consequently, these different sampling rates change the frequency response in each steady-state.

Now we turn our attention to the fixed controller design around 400 Hz. The proportional controller is modified to $G_P(s) = k = -0.1 \frac{V}{Hz}$ in order to lower the gain and stabilize the closed loop system. Adding an integral part to the controller is designed to have $\omega_c = 80 \frac{1}{s}$ getting the frequency control near the 6-dB sensitivity circle, yet at the same time keeping the frequency response above the Nyquist point to have an encirclement around it, thus keeping the system stable, $G_I(s) = 1 + \frac{80}{s}$. Thus, the final series implementation of the PI controller will be:

$$G_P(s) = k = -0.1 \frac{V}{Hz} \quad (5.2)$$

$$G_I(s) = 1 + \frac{\omega_c}{s} = 1 + \frac{80}{s} \quad (5.3)$$

$$G(s) = G_p(s)G_I(s) = -0.1 \left(1 + \frac{80}{s}\right) \quad (5.4)$$

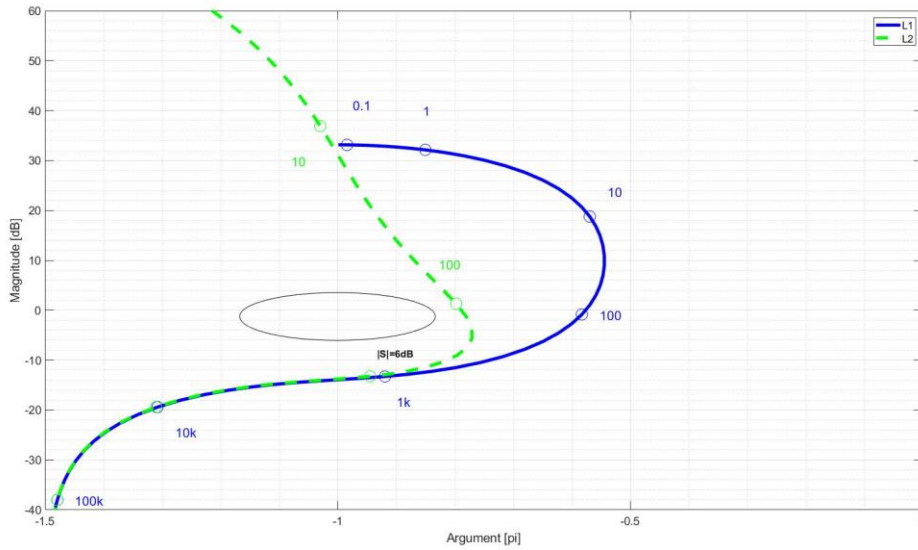


Figure 5.5: Loop frequency response at 4200 RPM. Blue line: L1 proportional controller added. Green line: L2 integral controller added.

Now looking at the system with different operating points we get the following results:

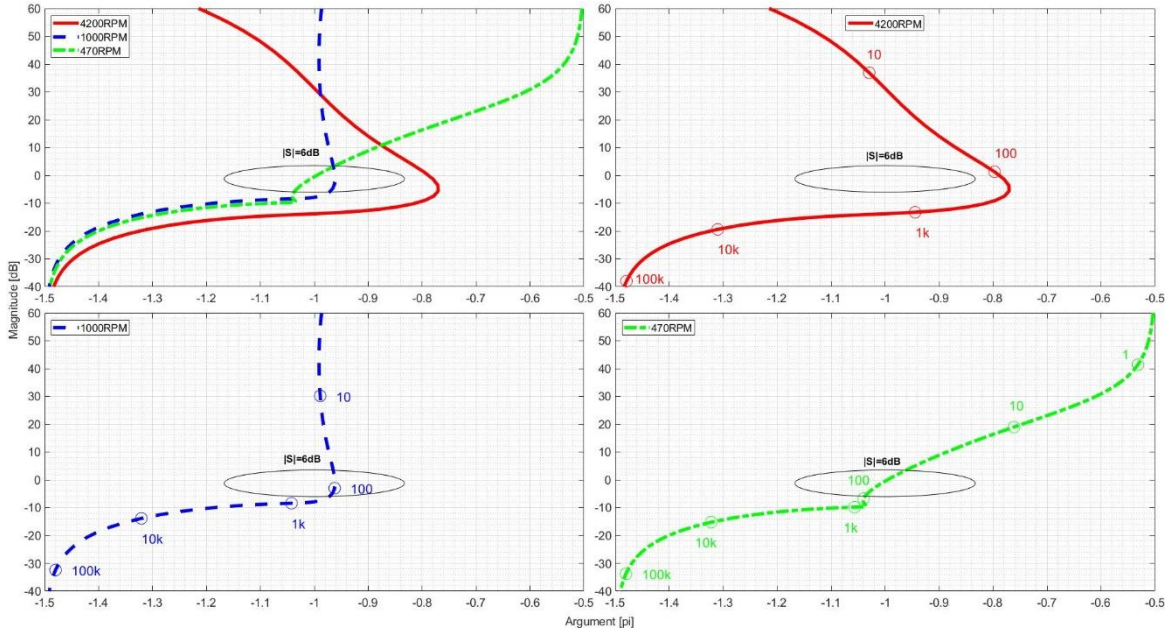


Figure 5.6: final frequency response with all effects added and the controller. Top left graph combines all the explicitly considered operational points, red solid line for 4200 RPM, green dash dotted line for 1000 RPM, and blue dashed line for 470 RPM. Top right graph, red line: L2 at the operating point of 4200 RPM. Left bottom: graph: L2 at the operating point of 1000 RPM. Right bottom graph: L2 at the operating point of 470 RPM.

In figure 5.6, the results show that for the working point of 4200 RPM the system is conditionally stable. The working point of 1000 RPM is too close to the Nyquist point making it almost unstable. Finally, the working point of 470 RPM is unstable, meaning the controller with the given parameters will make the unstable working points stable and the stable working points unstable. In conclusion, before letting the controller be active, the turbine must be operated manually, until it nears 1000 RPM (where it starts to be unstable in an open-loop), then switch to automatic control beginning with a lower gain than was designed and an increasing gain as the RPM increases. This kind of switch between manual and automatic is not necessarily bump-less since the controller at the beginning will have only a proportional part and the integral parameter will be zero. Also, the frequency reference is set to be close to the frequency right before the switch, which will cause a safer transition.

Up until now, the analysis and design are meant for stabilizing the system around the fixed point of 400 Hz. Although three operating points were considered, they are quite far one from the other. More operating points should be taken into consideration to make sure the uncertainty in the system will not affect the stability. Also, these operating points will be testing points in the actual runs, so it would be wise to check as well. There operating points will be 200 Hz and 300 Hz.

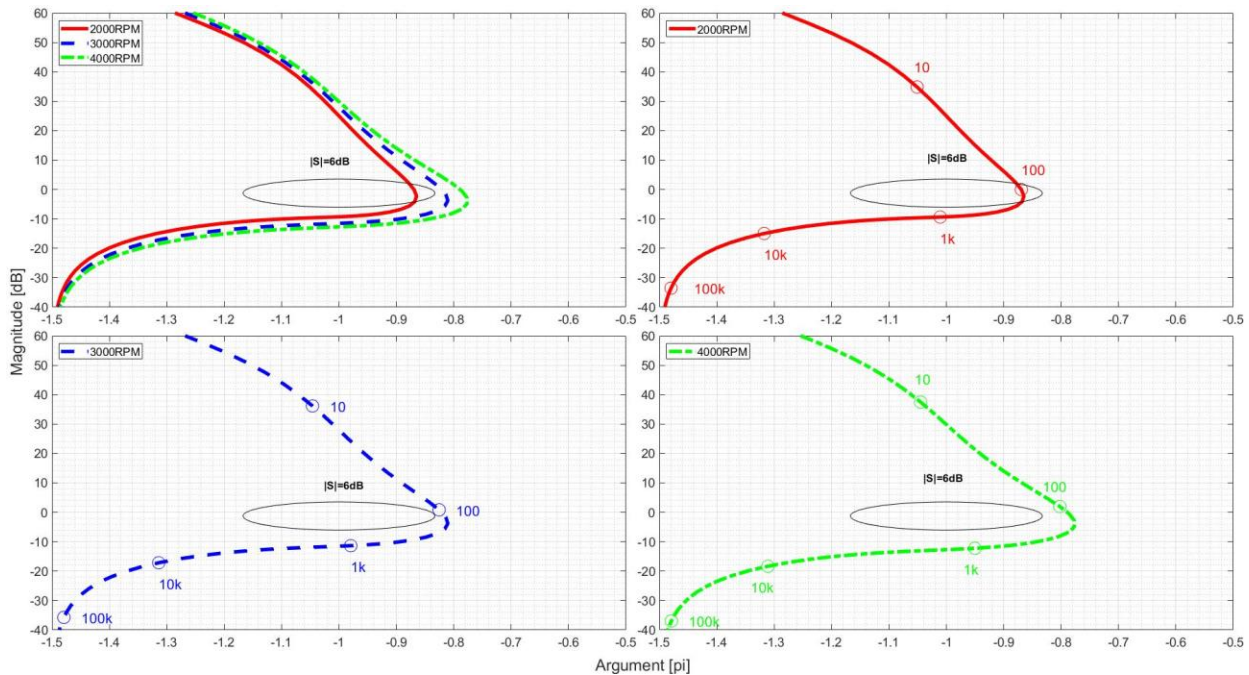


Figure 5.7: final frequency response with all effects added and the controller. Top left graph combines all the explicitly considered operational points, red solid line for 2000 RPM, blue dashed line for 3000 RPM, and green dash dotted line for 4000 RPM. Top right graph, red line: L2 at the operating point of 2000 RPM. Left bottom: graph: L2 at the operating point of 3000 RPM. Right bottom graph: L2 at the operating point of 400 RPM.

In figure 5.7, the uncertainty in the system, after it passes 1000 RPM, does not affect the stability of the system for the given controller in equation 5.1. Nonetheless, the system is still conditionally stable.

5.2 Controller implementation simulation

To check initially that the designed controller works in concept before physically implementing it, we will use Simulink software from MATLAB to simulate the non-linear model with the controller.

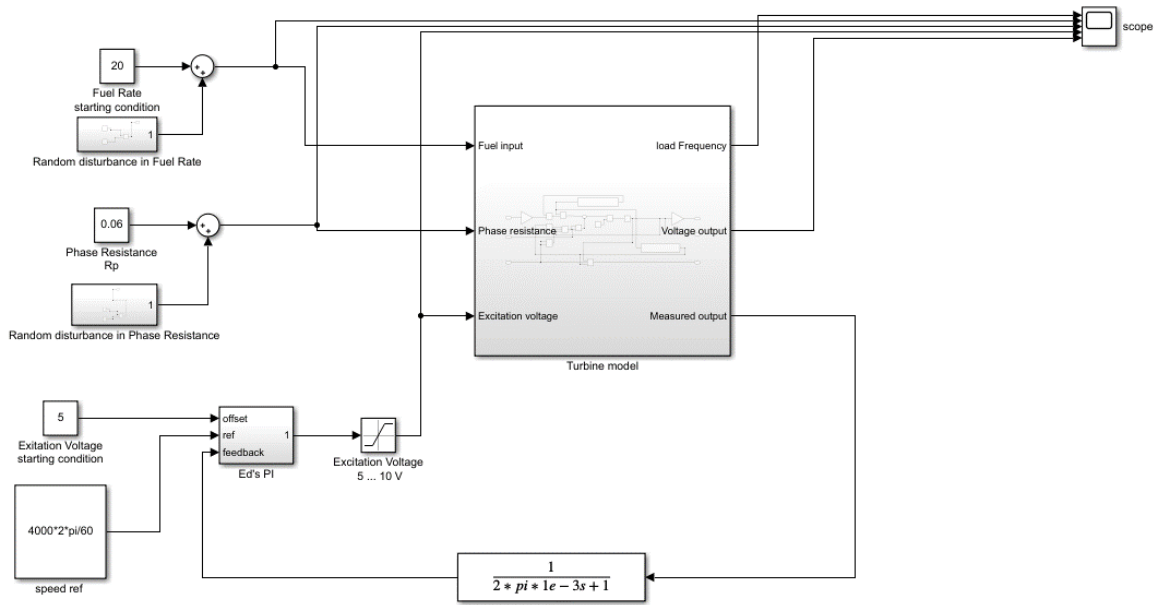


Figure 5.8: SimuLink implementation of the non-linear model with the controller.

The controller was made as a sub-model, as well as using Ed's proportional and integrational (PI) controller [14], which is a way of implementation developed by professor Eduard Eitelberg, where the PI controller is implemented in order to not let the integration calculation get to very high numbers, then if there is a change in the output the controller it will take more time for it to recalculate the numbers until we get correct values for the input of the plant. It is also called a reset wind-up controller, this controller is based on the discrete-time version of Shinsky [33]. The implementation of the controller is in the z-domain because the physical controller will be digitally implemented. The calculations for the series gain integral parameters in the z-domain for Ed's PI are taken from Eitelberg's control book [14].

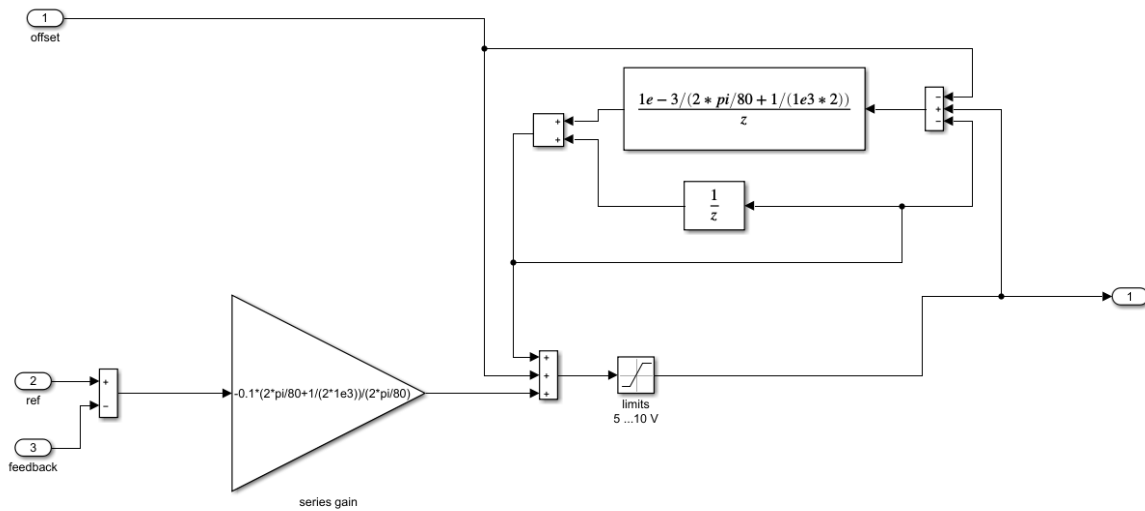


Figure 5.9: Ed's discrete-time PI.

The subsystem of the Turbine model is in figure 5.8:

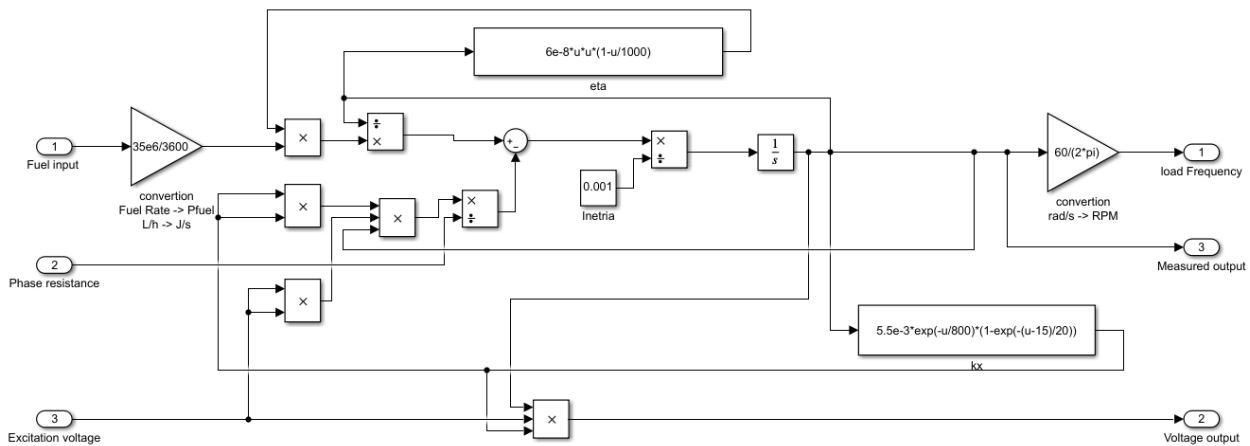


Figure 5.10: Non-linear continuous-time model of the turbine in Simulink.

The simulation is running near the working point of 4200 RPM. During the run we include a random change in the disturbance (change in the client's resistance), which will be made with step changes between 0.06Ω and 0.12Ω . Random changes in the fuel flow are also included in step changes. Change in the fuel flow means changing the working point thus modeling the uncertainty of the system.

5.3 Simulation results

This controller design is based on the linearized model that was developed before, based on the three operational points. Although the real model is non-linear, the implemented controller would start with the same parameters, then be adjusted to be fine-tuned during testing.

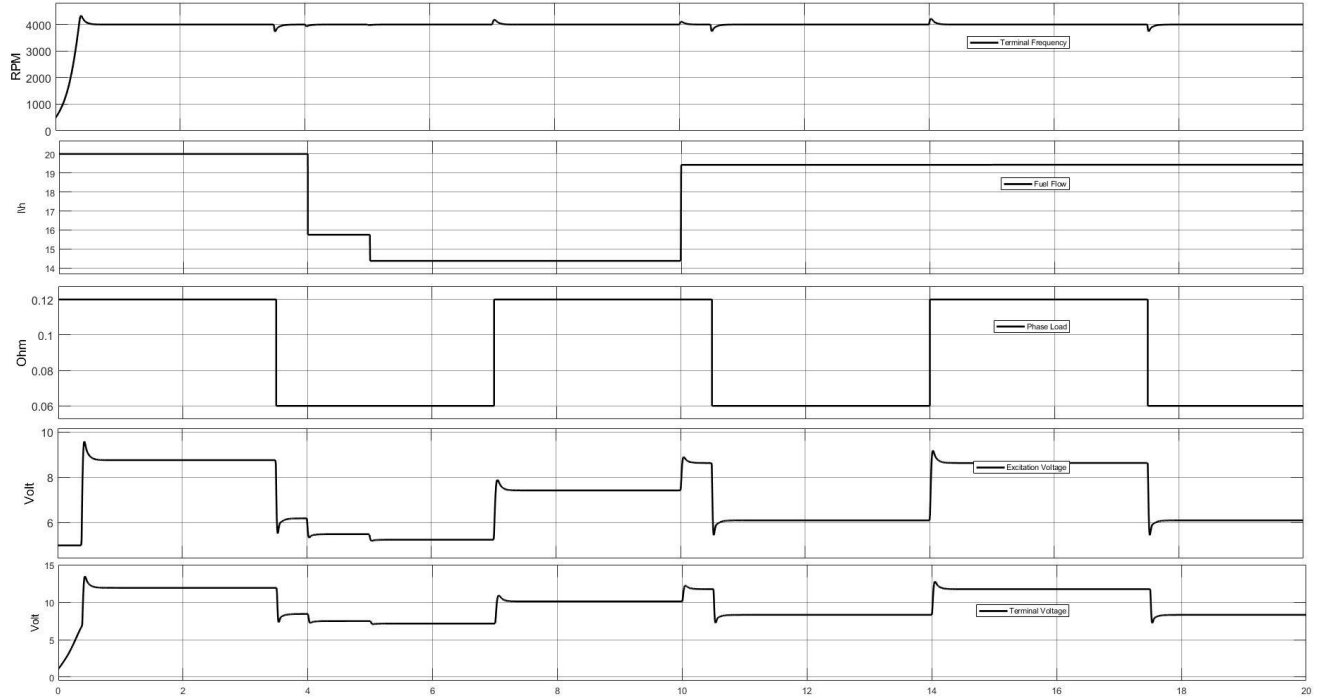


Figure 5.11: Signals from Simulink, from top to bottom: Rotor's RPM (RPM), Fuel Flow (l/h), Phase Load (ohm), Excitation Voltage (volt) and Terminal Voltage (volt). Horizontal axis in seconds.

The linear and non-linear models are now compared. The comparison is done mainly to show how the same controller regulates the output on each of the linear and non-linear controller. As for the linear model's parameters they are taken as in equation (4.37) to have the reference equal to 4200 RPM. On both linear and non-linear models there is an added delay in the feedback loop to try and predict how the sampling rate [4] will affect the output.

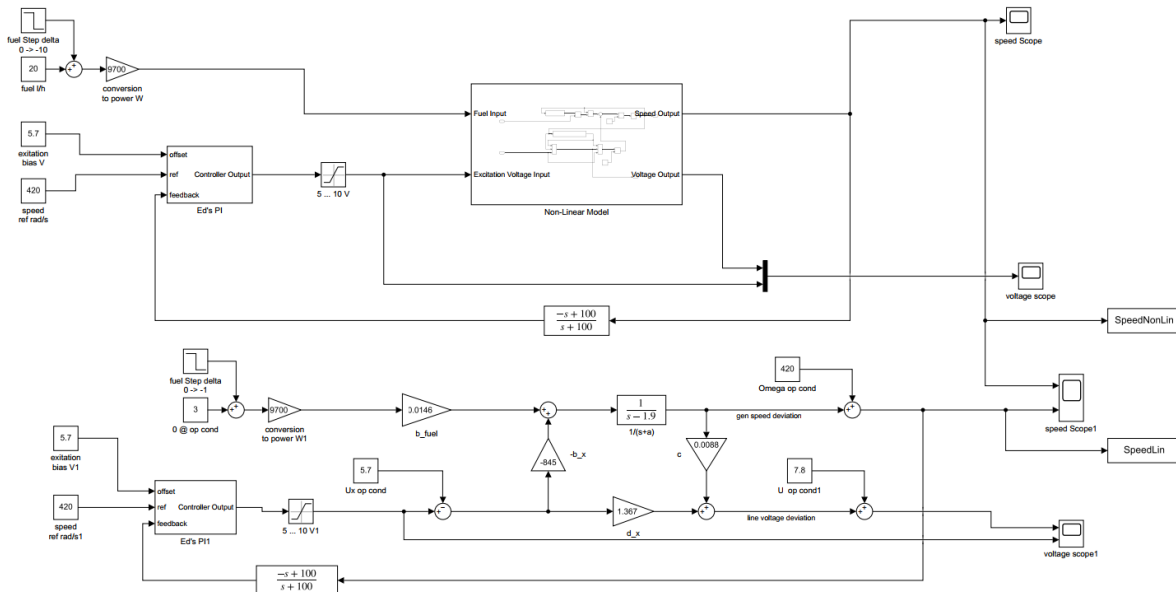


Figure 5.12: Comparison between linear and non-linear models. The upper side is the non-linear and the lower is the linear

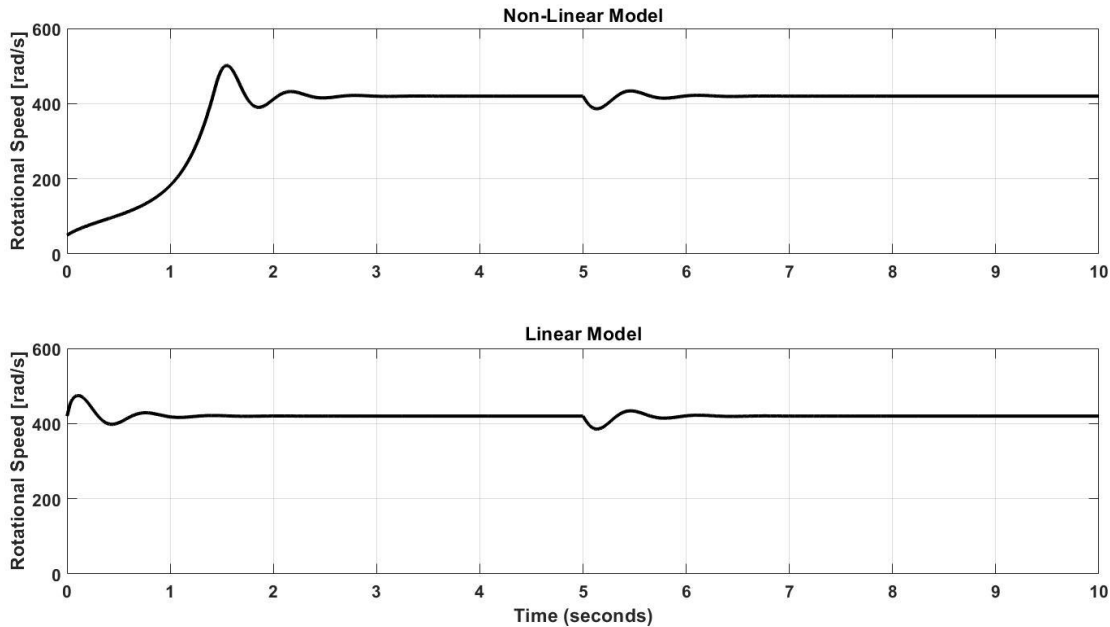


Figure 5.13: comparison between linear and non-linear models' outputs. The upper side is the non-linear and the lower is the linear.

In both models a disturbance has been added in the fuel flow at 5 seconds, thus making the rotational speed of the rotor decrease, yet the controller regulates the output the same in the linear and non-linear models. The linear model initial rotational speed is 420 rad/s, which is the point where the model was linearized. That is why the simulation for the linear model starts around the steady-state operational point and not from zero. Yet the nonlinear model starts from close to zero, as the real model measurements for the rotational speed starts from 150 RPM (15 rad/s).

5.4 Conclusions

The digital controller for the closed loop between the frequency (output) and excitation voltage (input) was modeled by taking first the effect of the sampling effect[4] on high frequencies according to a predefined frequency measurement function in the micro-controller. Then, both proportional and integral parameters of the PI controller were designed to stabilize the closed loop system for the generator's rotational speed greater than 1000RPM, where it was unstable in the open loop system.

Using Simulink software, the designed digital controller is implemented in the z-domain on the linearized model from section 4.3.4 with Ed's PI[14] of reset wind-up technique and was proven to be stabilize the closed loop system. Later a non-linear model was added as a comparison between linear and non-linear model to check the performance of the implemented digital controller, and the closed loop was also proven to be stable around generator's rotational speed of 4200RPM.

Next step in the research is to physically implement the digital controller using the micro-controller, using the design PI parameters in equations (5.2) and (5.3), and fine-tune both proportional and integral parameters it to the physical model.

Chapter 6

Controller implementation

To digitally implement the controller, we will use a micro-controller called the Teensy 3.6 [35]. This micro-controller is based on the Arduino language, yet it has better processing power as well as more versatile outputs and inputs. The output from the Teensy regulates the input of the turbine, and the controller's output signal is chosen to be in the form of a pulse-width modulation (PWM) signal. The two main reasons for choosing PWM over pulse-amplitude modulation (PAM) are better power efficiency as well as better immunity to noise. As for the output signal of the turbine, we will measure it and process it inside the controller.

6.1 Hardware implementation

Before getting to the digital controller's calculation and implement then into Teensy 3.6 micro-controller, there is a need to adapt between the signal from the process's output –the generator's electrical frequency– to the input of the micro-controller, as the generator's supply voltage produces a sinusoidal wave with a magnitude up to 13.1 V while the micro-controller's input range is between 0 V and 3.3 V. There is also a difference between the voltage ranges between the micro-controller's output to the input of the process – the generator's excitation voltage –, the micro-controller's output voltage range is between 0 V and 3.3 V while the generator's excitation voltage is between 5 V and 10 V. this means that there is a need to design electric circuits to convert the volt ranges in both cases:

- 1) Reducing the amplitude from the generator's supply voltage and shift it up to be not symmetrical around 0 V then feed it to the micro-controller input, in order to not burn the micro-controller. more details are described in section 6.1.2.
- 2) Amplifying the voltage of the micro-controller's output and feed it to the generator's excitation circuit, to ensure a function for the excitation voltage. more details are described in section 6.1.4.

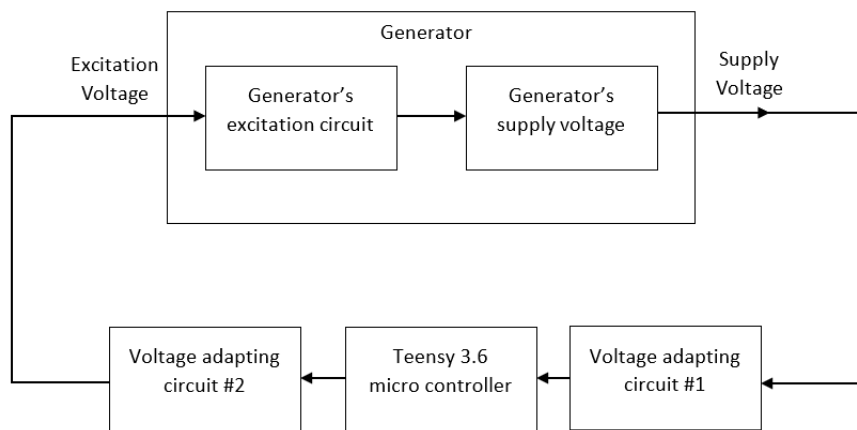


Figure 6.1: closed loop system with micro-controller and adapting circuits.

6.1.1 Measuring the load's frequency

We are measuring only one parameter of the process's output, which is the generator's frequency, that usually means lower complexity in the algorithm of the micro-controller and electronic circuits mentioned in section 6.1, to have a reliable measurement, but this system had excessive of noise that had to be dealt with at various levels to overcome it. The noise was generated due to the nature of the system, which may

be caused by the numerous transformers installed in the system or the generator itself. Also, the micro-controller was placed far from the turbine while operating and testing the controller safely, and long cables were connected to have a safe distance. The longer the cables, the more noise was added to the measured signal. Since the generator is a 3-phase generator and the loads are identical, it suffices to measure the frequency on one of the phases only to regulate it. Even with the load disturbances, the three phases will remain identical.

6.1.2 Frequency measurement circuit design

The voltage generated from the generator will be used to measure the generator's frequency. The electrical signal will need to go into the controller to analyze the data. This is the first aspect that needs to be dealt with because the generator output voltage is a sinusoidal wave of amplitude between 0V to 13.1V (generator operating points between 0 to 10k RPM), while the controller's analog to digital converter (ADC) input may only withstand voltages in the range of 0V to 3.3V. Not only is the generator's voltage greater than what the controller may receive, but part of the signal is also negative. Since there is additional noise and a maximum of 13.1 V output voltage only at the operating point of 10k RPM, the measuring circuits were designed to deal with ± 15 V out of an abundance of caution to avoid the inclusion of fuses or additional protection elements or circuits.

Returning to the generator's signal, the pure sine wave with a maximum amplitude of 15V was designed to be a sine wave that is limited between 0 and 3.3V. To do that, an offset to the signal should be added and the amplitude should be reduced as well. Naturally, the offset needs to be in the middle of the range to enable a maximum swing of the sine signal. If the offset is not in the middle, the measuring circuit will need to clip the signal, get into a non-linear operation condition, or reducing it even more to keep the pure sine signal, but it will make the smaller voltages be even smaller and then more prone to noise. Thus, leaving the offset at:

$$Offset = \frac{V_{Max} - V_{Min}}{2} = \frac{3.3 - 0}{2} = 1.65 V \quad (6.1)$$

Because the signal will be centered at 1.65V, it can get an additional ± 1.65 V until it reaches the limits. So, the amplification will be calculated according to the maximum voltage that we may receive (15V) and not only around the main operating point.

$$Amplification = \frac{V_{Modified Max}}{V_{Turbine Max}} = \frac{1.65}{15} = 0.11 V/V \quad (6.2)$$

Implementation of these two functions may be done with operational amplifiers as they are more than sufficient for such a function. The circuit will be designed using three operational amplifiers (Op-Amp), all supplied with ± 15 V from an external source. Also, the ground is connected to the neutral point of the three-phase load.

The first Op-Amp will be an inverting amplifier to reduce the maximum amplitude from 15 V to 1.65 V, an inverting amplifier is used to reduce the amplitude, and the phase switch does not affect us as we are measuring frequency.

The second Op-Amp will also be an Inverting amplifier to get an accurate offset of 1.65 V. To do so we will feed the Op-Amp input with constant 3.3 V output from the controller. Since it is inverting and the input to the amplifier is positive, the output will be -1.65 V. This is not a problem as we will solve it in the last step.

The third Op-Amp will be a summing amplifier. These amplifiers have multiple inputs, while one can configure each amplification of input as well as add a negative sign. That way, both offset and reduced sine wave will be added, while simultaneously having a positive offset.

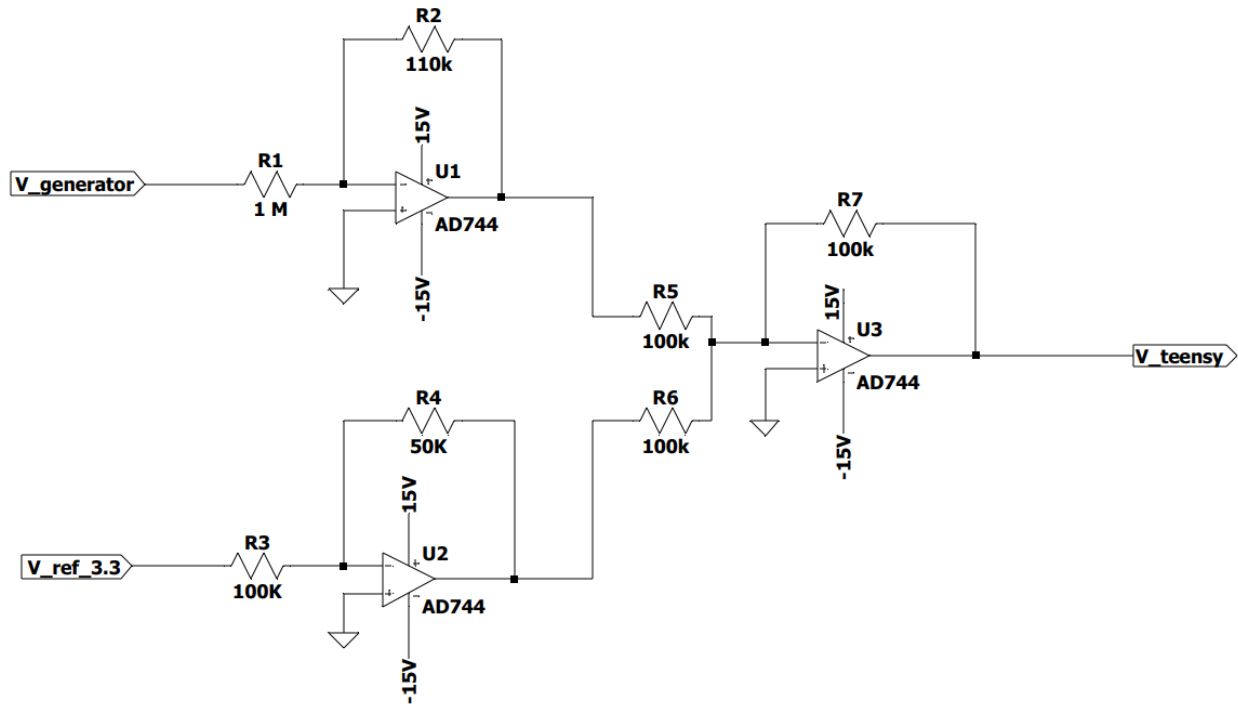


Figure 6.2: measuring circuit.

As mentioned before, the generated noise was interfering strongly with the signal. When this circuit was designed and implemented at the beginning, it was connected to the loads and was placed very close to it. Under these conditions there were almost no problems. There were some deviations in the frequency measured by the microcontroller after receiving the signal. To solve this problem, a moving average was added to the code and thus giving a better measurement.

Due to safety of moving near the turbine system, the controller was moved further from the turbine, but this reallocation created two additional measurement noises, small jumps in the signal, and some sudden peaks. These two problems would give us false information about the measured frequency. For instance, if we measure the load's frequency using an oscilloscope it would be 100 Hz, but if we take the controller farther from the turbine (load) it can measure 100 Hz if there are no jumps or peaks, 120 Hz if there is a small peak, or even a sudden 3000 Hz from the peaks. To solve the first problem of small jumps, the first Op-Amp was changed from inverting amplifier to a Schmitt trigger with the thresholds at 0.25 V. Although the measured signal in the controller would not be a sine wave, but then again, we are regulating frequency.

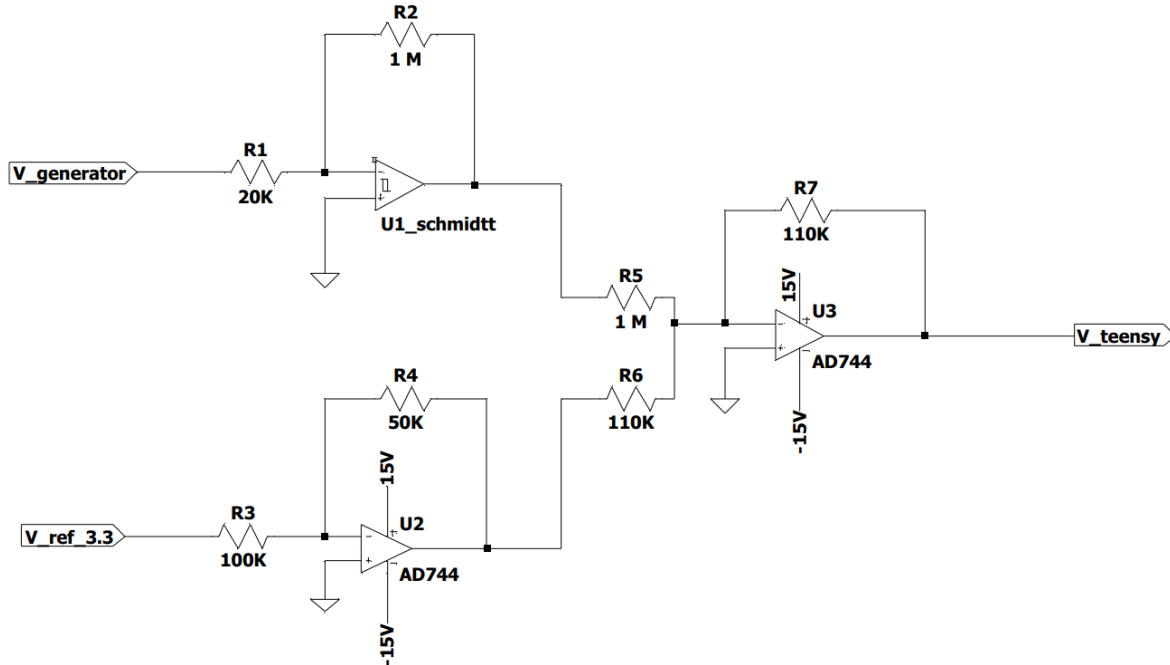


Figure 6.3: measuring circuit with Schmitt trigger connected to the generator output.

As for the peaks, a first-order low-pass filter was added to the input of the Schmitt trigger as well as at the input of the controller. The corner frequency is designed to be 1 kHz, that way it does not affect the design in the desired frequencies, as it will lower the magnitude and introduces lag of frequency response of 6.3 k rad/s in figure 5.7, which does not affect the stability of the closed loop system.

This method of measuring the frequency from the generator to the microcontroller might not be the most efficient way. But, this design was sufficiently good, as the main bottleneck in measuring the electrical frequency, which introduces lag, is from the microprocessor's ability to process the frequency measurement, which is already taken into consideration at section 5.1.

6.1.3 Regulating the generator's excitation voltage

As in the previous section (measuring the frequency), we are using a high-power system with an electronic system. Furthermore, changing the excitation voltage cannot be done directly by connecting cables to the coil surrounding the rotor. To do so we would need to design a circuit to amplify the PWM output of the controller to get the required voltage, as the controller's voltage is between 0 to 3.3V while the excitation voltage is between 5 to 10V. Another solution would be connecting a motor for physically moving the excitation handle, but it would be not as accurate as an electronic design.

6.1.4 Regulating the generator's excitation voltage circuit design

To manually change the excitation voltage, we would need to move the lever. The lever is connected to a potentiometer that changes the voltage/current going through a transformer to change the high AC voltage to low voltage. The secondary side of the transformer – the low voltage between 5 to 10 V – is connected to a diode bridge with a capacitor to change the AC to DC and then to continue to the rotor.

It would be wiser to connect the new circuit not only to the secondary side of the transformer as well as after the bridge. A switch will be placed also to let the user have the option of either manually change the excitation voltage or let the automatic process of the controller start working. As for the connection between the controller and we will use the following circuit:

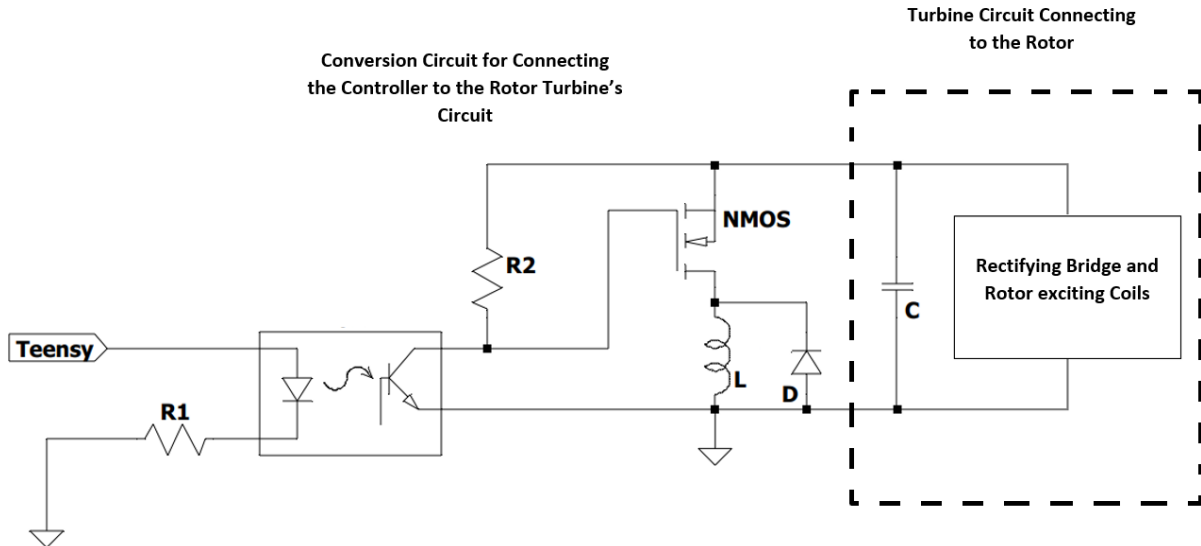


Figure 6.4: connection from the micro-controller to the exciter.

Its main function is to separate the circuits as well as amplify the signal to be in the required range. The supplied voltage to the transistor will be from the filtered signal after the bridge (10V). That way the PWM connected to the amplifier will be between 0 to 3.3V and the output will be between 0 to 10V and up to 20A, using the duty cycle we will change the excitation voltage accordingly. Also, the coil L in figure 6.4 is meant to keep the current flowing in one direction to protect internal system circuits, and since the transistor will be in cut-off (because it is working as off and on switch for the pulse width modulation) this coil cannot be in an open circuit we connect a diode to it.

6.2 Software implementation

As for the digital part, the micro-controller's code is divided into four main parts. Each part is a function that is coded to work in a serial part, other than the PWM output. The PWM output works as a stand-alone peripheral that only receives the parameter of duty-cycle, modifies the output and continues working regardless of the calculations made by the micro-controller or any other function working.

6.2.1 Frequency measurement of the generator signal

The micro-controller in use (teensy 3.6[35]) has a built-in frequency function, the author used it here to measure the converted signal from section 6.1.4. The built-in frequency function in the micro-controller measures how much time elapses for each cycle and returns the frequency to the user. The data collected may contain some noise, and in to reduce it the author averaged 6 samples (6 cycles) to have a more accurate measurement.

This built-in function is called FreqMeasure, and according to the specifications of the manufacturer, it is well suited for frequencies between 0.1 Hz and 1 kHz. FreqMeasure suffices for the given generator as the frequency can go up to 1 kHz, if the generator surpasses 1 kHz the system will perform an emergency shut-down, as well as the aim is to stabilize around 400Hz.

The only issue with using FreqMeasure is it can not measure 0 Hz, which makes sense as it will take infinite time to complete a whole cycle, in such case the micro-controller will get “frozen” as it awaits data from FreqMeasure which will never arrive. To overcome this issue, the author added to the micro-controller code a timer, where if FreqMeasure is stuck for more than 0.1seconds it will conclude that the frequency is 0, as the controller is supposed to work in generator’s frequencies between 100 Hz or greater, and while the generator’s frequencies below 100 Hz the system will be controlled manually.

6.2.2 Implemented Algorithm

After the frequency is measured in each cycle, the algorithm of the controller will decide the output of the PWM using the parameters of gain and integral parts. Also, for safety measurements, the code does not allow the PWM to go below 50% duty cycle (excitation voltage 5V), nor to drop below the factory’s minimum voltage design, nor will it go above 100% duty cycle (excitation voltage 10V) because of the Ed’s PI controller design. Without this it would presumably wrap to an incorrect value if the PWM command input is above 100%. The algorithm is based on the following diagram:

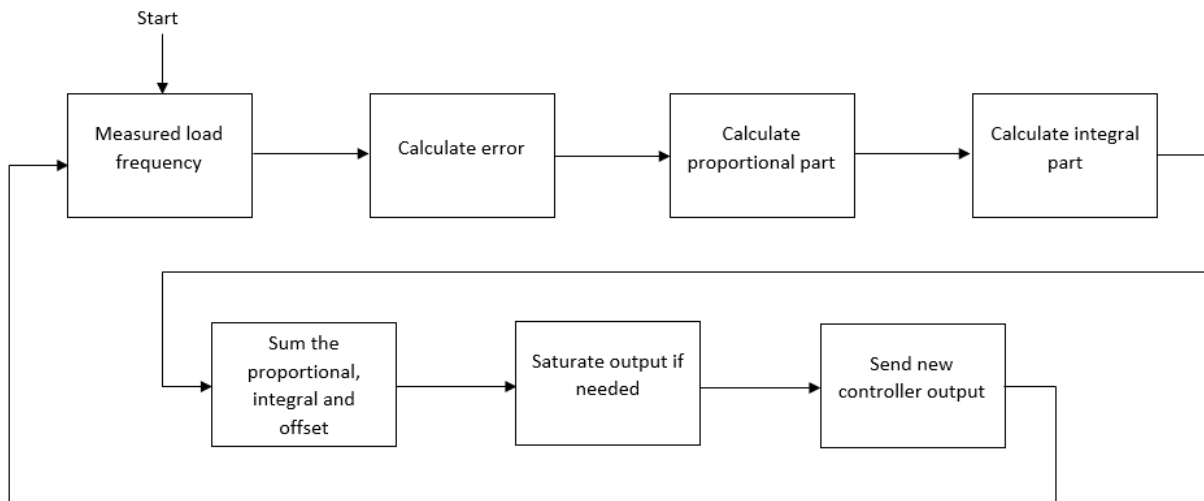


Figure 6.5: algorithm flow.

The initial parameters are prefixed, but the user is able to change them.

6.2.3 User input to control parameters

The user can have control over various parameters in the controller. The parameters are:

- 1) Reference: the reference is the required frequency output from the generator. The default is 400 Hz, but it can be changed to anything between 15 Hz to 8 kHz. That way the user will not have the option to set the reference to be 10 kHz or more.
- 2) Gain: the gain is the first part of the controller. The default is -0.5, but it can be changed to any negative number including zero. At first, for testing purposes, it could be chosen to be positive, but as seen in the frequency response in chapter 5, the gain should be negative to stabilize the system.
- 3) Integral Corner Frequency: the gain is the second part of the controller. The default is 10 but can be changed to any positive number, as there is no logic to a negative number.
- 4) PWM operational point: it is the main operational point of the PWM output that should workaround as the controller will be fixing the error to regulate the generator’s frequency. The

default is 50% duty cycle, so even if the user begins with zero gain and integral corner frequency the PWM will work within the limits.

- 5) Output delay: the code should not change the PWM at the end of every loop, as it will be faster than needed and the frequency of the generator will oscillate instead of being constant, especially around 400 Hz.

6.2.4 Data logging

To make sure that the controller is working correctly, a logging function was added. The author could not rely on the manufacturer's logging software primarily because it would not record the microcontroller's calculations, but also, the manufacturer's software has a limitation of a maximum of 10 samples per second. The logging function will log the following parameters:

- a. controller's gain
- b. controller's integral corner frequency
- c. output delay time
- d. PWM operational point
- e. Measured frequency
- f. Reference
- g. The error between the reference and measured frequency
- h. Proportional calculation of the controller
- i. Integral calculation of the controller
- j. The duty cycle of the PWM

6.3 Disturbances creation

To see how we overcome disturbances in the system we will create them manually. The first disturbance is the fuel flow change, as the system is stable around a certain frequency. If the fuel flow drops, then the generator's RPM will drop also, and vice versa. The second disturbance in the system will be the resistive load. A switch is installed to either have a resistive load of 0.12Ω or half it manually to 0.6Ω . If the resistance drops, then there is more load on the generator meaning the RPM will drop, and vice versa.

Chapter 7

Practical Aspects and Results

While running the turbine there was a difference between the theoretical model and the actual system. First trials with the controller started the turbine in manual mode. After making sure the system is running well, the automatic control mode (from figure 6.4) was initialized by using only the proportional part (the integral part was disabled) and feeding the electrical frequency back to the controller and manipulate the excitation voltage. This was very successful as we were able to get a stable result even with different reference values. The author also tried to change the fuel flow and the load value to create disturbances, yet the system stayed stable. The second phase of trials was the addition of the integral part, to eliminate the error as much as possible. The following graph was created from the logged data in the micro-controller from one of the final runs, but unfortunately, the system had a malfunction, and the generator overheated. Thus, the system cannot start up again.

7.1 Frequency control results in a closed-loop system.

the controller was implemented without a reset wind-up protection as intended in figure 5.9, but as an academic series form PI controller. It was intended to be this way to start with a simpler code to have a proof of concept that the controller works, then implement the controller as in figure 5.9.

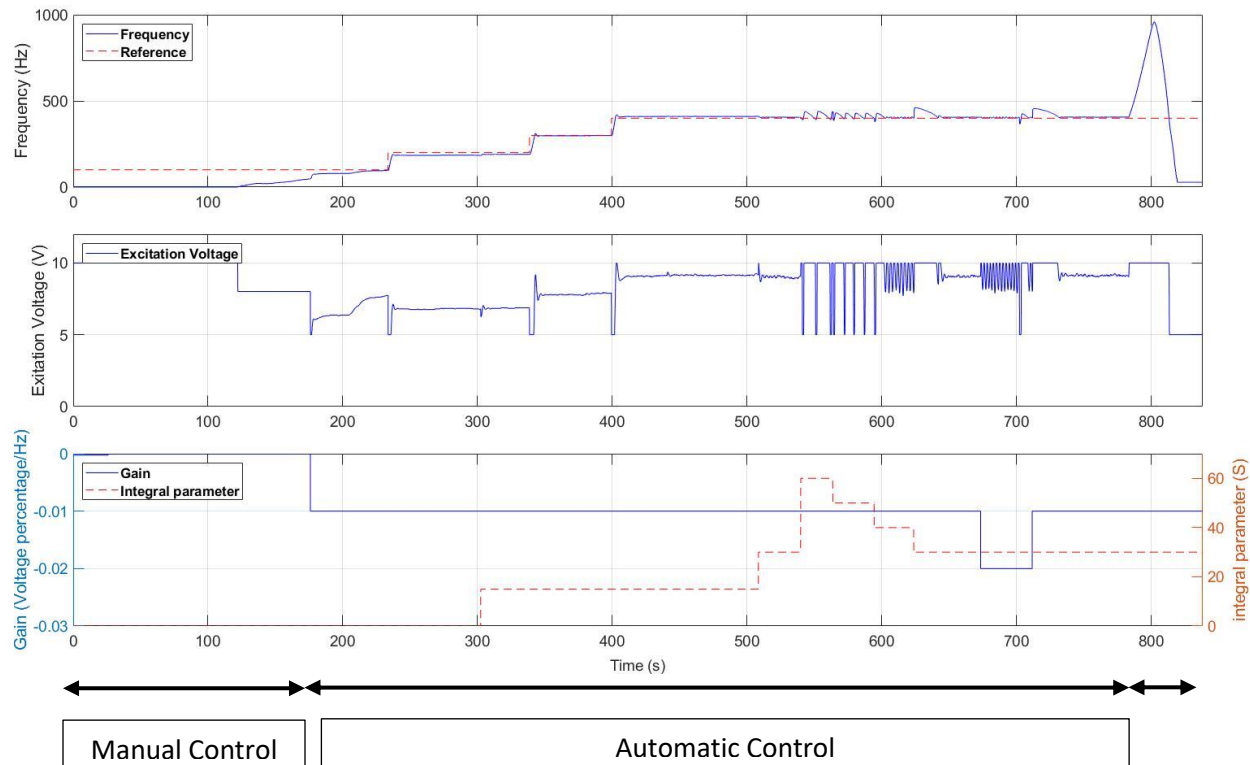


Figure 7.1: Electrical measurement with the controller. Upper graph blue solid line: measured frequency (Hz). Upper graph red dashed line: reference (Hz). Middle graph blue line: excitation voltage (V). Lower graph blue line: gain (voltage/Hz)(eq. 5.1). Lower graph red dashed line: integrator corner frequency ω_c (rad/s)(eq. 5.2).

In the first part of the run, the system was controlled manually. After that, it was switched to automatic mode (the controller was turned on) with only proportional control with reference of 200 Hz, 300 Hz and then finally 400 Hz (r_1 , r_2 and r_3 respectively). The sudden peak at the end of the run around 800 s occurred because the control was changed from automatic to manual. Since at this operating point the system is unstable, it can be observed that the generator RPM accelerated until the system automatically shut down. The proportional control was stable even around 400Hz with small error as seen in figure 7.1.

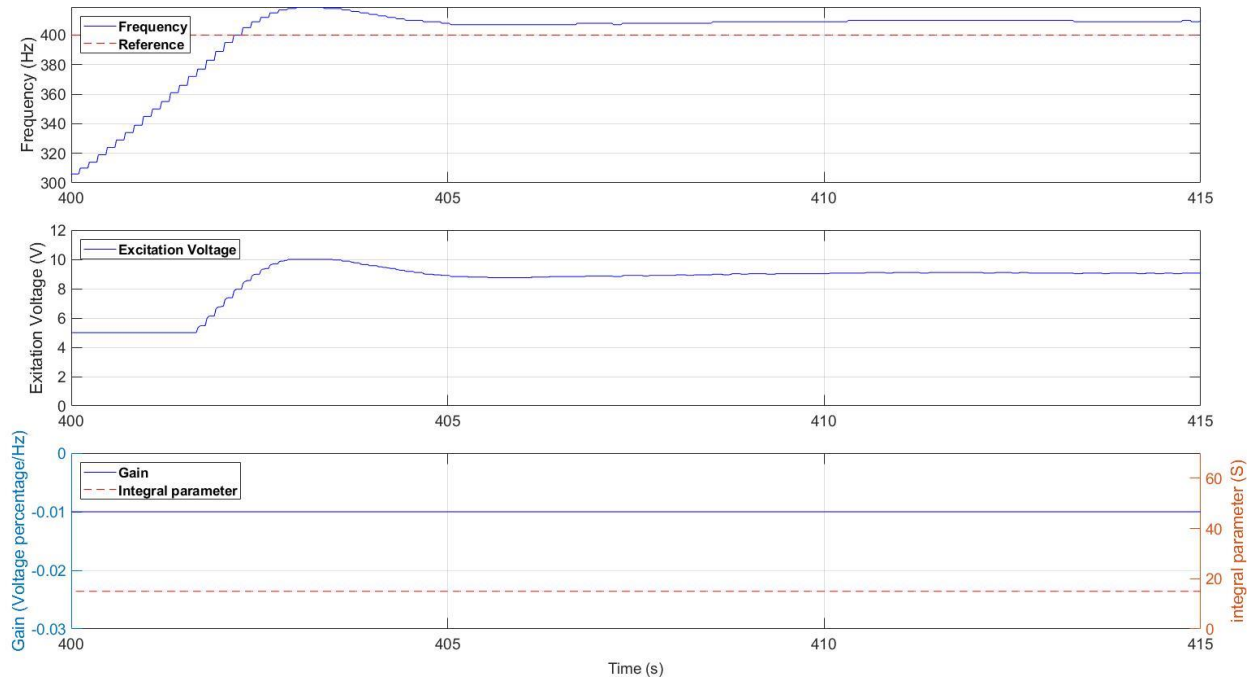


Figure 7.2: close up at when the reference was changed to 400 Hz. Upper graph blue line: measured frequency (Hz). Upper graph red dashed line: reference (Hz). Middle graph blue line: excitation voltage (V). Lower graph blue line: gain (voltage/Hz)(eq. 5.1). Lower graph red dashed line: integrator corner frequency ω_c (rad/s)(eq. 5.2).

The error between the reference and the measured frequency is $e = 10 \text{ Hz}$. Since there was no specification for the maximum allowed error we cannot say if it is good enough or not.

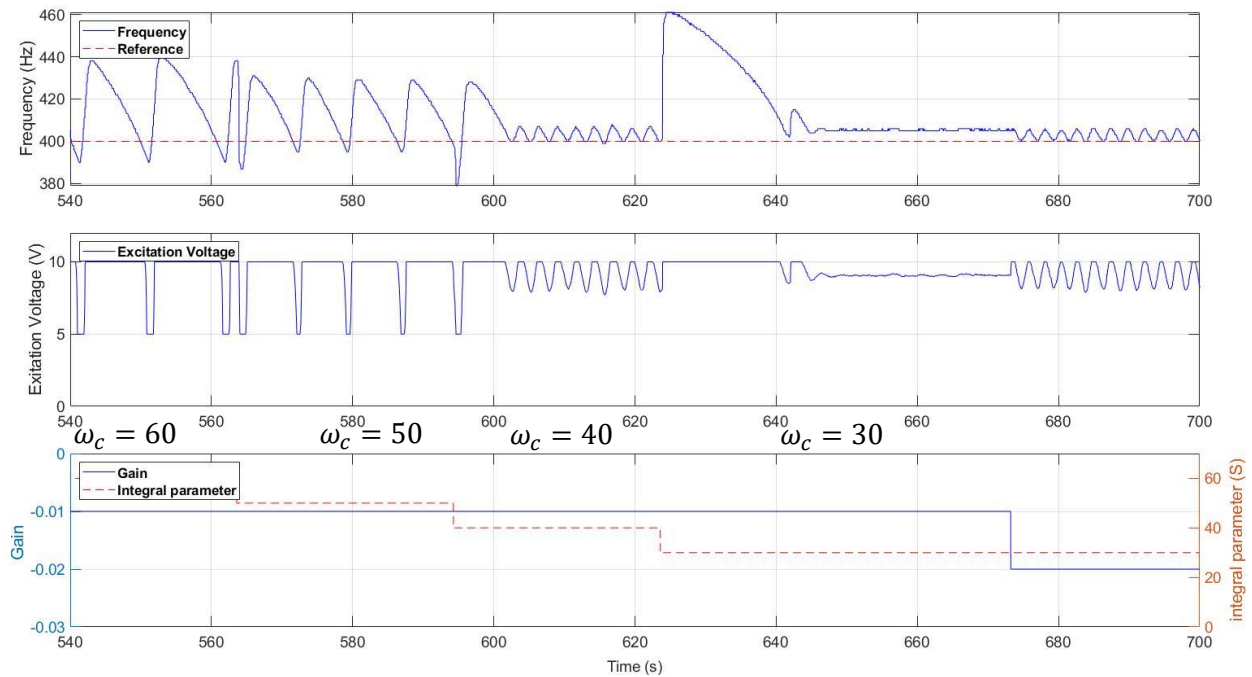


Figure 7.3: Electrical Frequency measurement, the reference is 400Hz and various corner frequencies for the controller integration parameter. Upper graph blue line: measured frequency (Hz). Upper graph red dashed line: reference (Hz). Middle graph blue line: excitation voltage (V). Lower graph blue line: gain (voltage/Hz)(eq. 5.1). Lower graph red dashed line: integrator corner frequency ω_c (rad/s)(eq. 5.2).

The oscillations observed in figure 7.3 are called a limit cycle, which are stable in the implemented system. The fact that the amplitude of the cycle changes as the corner frequency of the integral part of the controller is changed, means that this behavior is caused from the non-linearity in the system that could not be investigated because the system broke down. Yet it can be seen with an integral part of 30 and gain of -0.01 the system would be stabilized without exhibiting a limit cycle. Another problem that is presented in figure 7.3 is the average frequency in each state. Because of the integral effect, the output should asymptotically go to the reference, yet there is a small error. This might be caused by inaccuracy in the measurement.

7.2 limit cycle comparison between experimental results and simulation

As mentioned in the beginning of the chapter, these trials were one of few runs with the controller implementation before it overheated and broke. In these measurements the controller was not implemented as Ed's PI controller (reset wind-up protection), but as gain multiplied by an integral which created the limit cycle. Even though the system is malfunctioning, the same effect of the limit cycle is proved to be from the controller implementation using the non-linear model simulation. The following simulation figure differs from figure 5.8 by multiplying the efficiency coefficient (from equation 4.21) by 1.5, multiplying k_x coefficient (from equation 4.22) by 0.8 and having the first 10 seconds using the reset wind-up controller then linear controller.

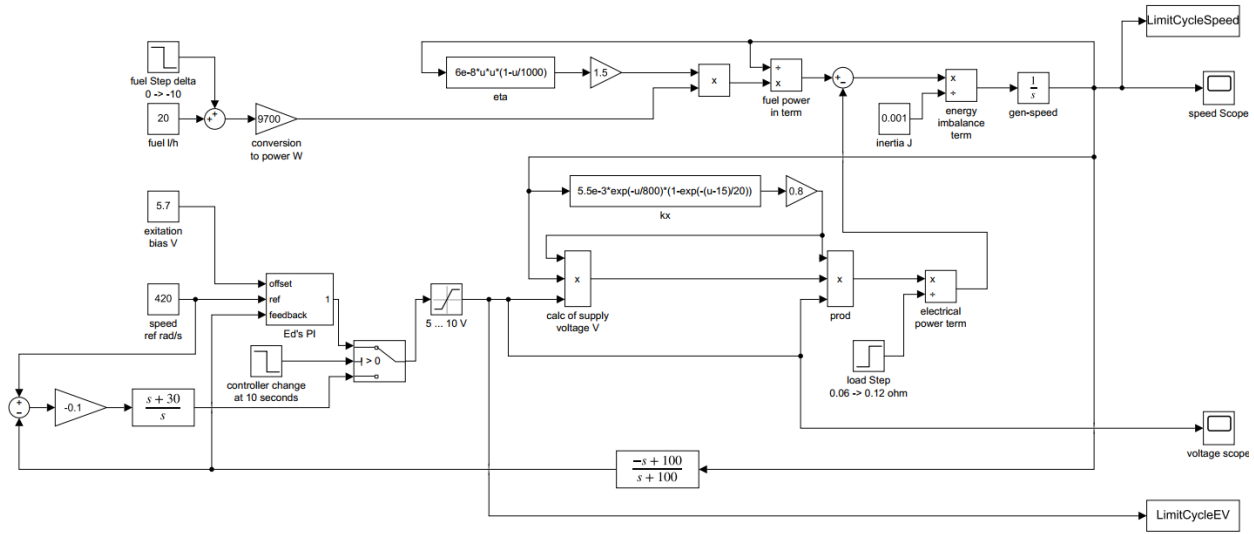


Figure 7.4: Non-linear model with two controllers to show limit cycle.

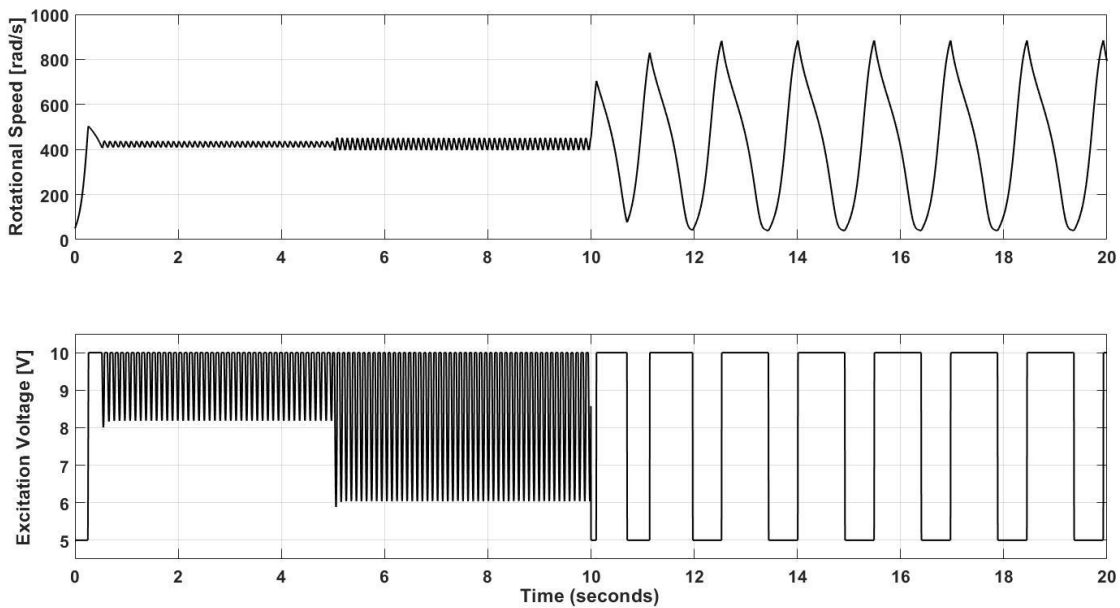


Figure 7.5: rotational speed of the rotor and excitation voltage in the non-linear model using two controllers.

In figure 7.5 it can be seen between 0 and 10 seconds the system is stable by the reset wind-up controller with upper limit cycle that behaves as the experimental result's limit cycle but with different frequency. After 10 seconds the controller is changed to the series PI controller where the system is unstable with limit cycle, yet this limit cycling has the same frequency as shown in figure 7.3 in the last part. Regarding the rescaling of efficiency coefficient and k_x coefficient to match the experimental results, either means that the theoretical model is accurate but needs some modifications, or that the system has been worked over 3 years without maintenance thus changing its characteristics.

7.3 conclusion

The system has been successfully operated at a frequency close to 400 Hz. During these trials, the turbines suffered some damage, probably from overheating. The overheating is suspected to be due to long operation of the generator at 4000RPM, as both manual and experiment document for turbo-gen[1] has been written and intended to be below 1000RPM. Furthermore, the factory test conducted for the system sent to OBC contains graphs and figures of multiple parameters, one of them is the generator's RPM.

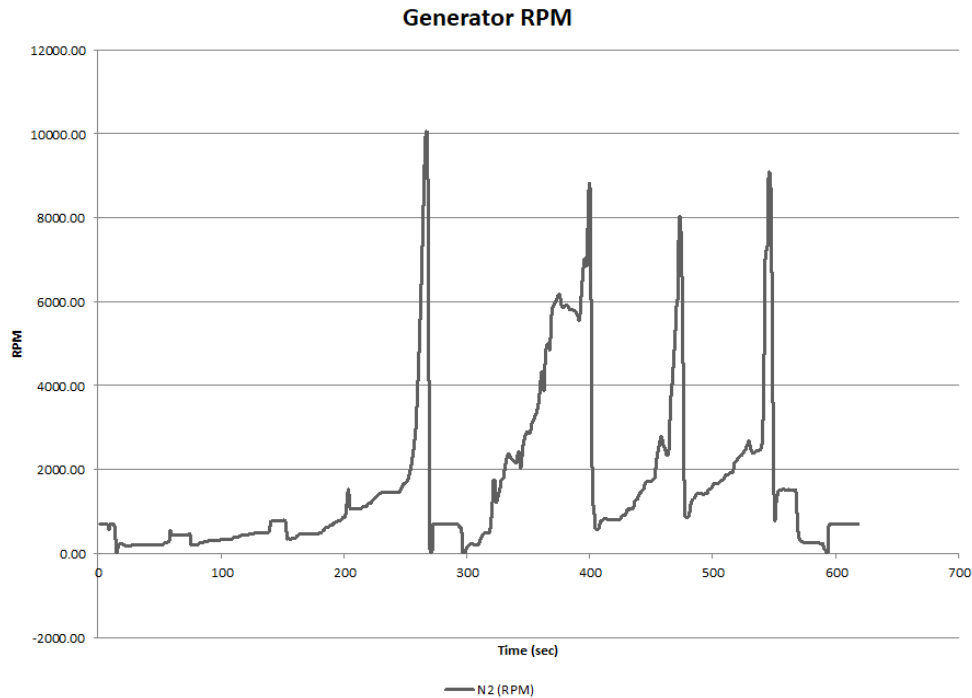


Figure 7.6: Generator RPM factory test by TURBOGEN[1].

In figure 7.6, the factory test has operated the generator with rotational speed greater than 1000RPM for less than two minutes cumulatively, while the longest it has operated in the mentioned range is approximately a minute. Then, the generator did have windows of time to cool down. Comparing to the latest run done by the author in figure 7.1, where the generator has operated with rotational speed greater than 1000RPM for more than nine minutes consecutively. Thus, the generator did heat without any time window to cool down.

Unfortunately, the turbo-generator can no longer be operated, as it shuts down automatically after a few seconds of starting it up. Further testing of the designed PI control system is not possible in the near future. Fortunately, we have recorded enough data to prove the design concept.

Chapter 8

Conclusion

The aim of this research was initially to design and implement a 2×2 control system, to regulate the terminal voltage and frequency through the use of fuel flow and excitation voltage. The first step of a multivariable design should start with analysis of plant interactions. The measured and calculated interactions were so strong that it was impossible to control both outputs within the given scope of the inputs. Thus, with the given range of both inputs (fuel flow and excitation voltage), the only option left is SISO control system.

In the analysis of the system, it was found that there is a pole that shifts from the LHP to the RHP according to the operating point of the frequency. The pole is in the LHP during the narrow range of 15~100 Hz of electrical frequency. At the rest of the range of 100~1000 Hz (electrical) the pole shifts to the RHP making the system unstable. This kind of operation is not trivial for these kinds of systems, as they are meant to be operated for applications, such as airplanes or ships, with frequency of 400 Hz.

During the analog design of the control system, while keeping in mind the uncertainty of the plant, it was found that while the pole is in the LHP, the controller would make the system unstable, but when it shifts to the RHP, the controller stabilizes the plant. To overcome this problem, the Turbo-Gen was started manually without feedback control until 100 Hz. If one wanted to close the loop, he should first exceed the 100 Hz and manually close the loop. In real life usage, this kind of switch should be programmed to be done by the micro-controller automatically, but this kind of system is unlikely used in the marked for its instability above 100 Hz.

It is common in designing a digital controller, first to design the analog controller, then estimate the sampling rate by multiplication with the transfer function of $1 - sT/2$ and choosing the T (sampling time) accordingly, to keep the system stable. The digital implementation affects the behavior of the high frequency range, while in the low frequency it is neglectable. But the microcontroller used in this dissertation already has a built-in function that is used to measure the frequency which gives a constant sampling time per frequency. To do the design, the author had to first take into consideration the sampling effect first and then design the PI controller. The author stabilized the system with small oscillations that required some fine-tuning to get a better result.

Also because of this system's nature, where only a small portion of the thrust from the jet engine is used to drive the generator, it could be taken as a concept of generating extra electrical power in an airplane. Also, it could be considered as a safety feature in airplanes, in a scenario where the battery is malfunctioning the generator uses a small portion of the thrust to create electrical power. That is the main reason why the frequency was stabilized around 400 Hz.

Even though the system is malfunctioning, and the college may not be able to fix it in the foreseeable future, it was interesting to analyze the system, to see how the uncertainty changes the behavior of the system from stable to unstable, and stabilize it despite the fact that it should inherently be stable near 400 Hz for these kind of applications.

Bibliography

- [1] Gas Turbine Electrical Generation System TurboGen™, Online, "<http://www.turbinetechnologies.com/Portals/0/pdfs/specifications/TurboGen%20Specs.pdf>".
- [2] P Kundur, Neal J Balu and Mark G Lauby, "Power system stability and control". McGraw-Hill, Inc., 1993
- [3] Edward Boje, Osita Nwokah and Glenn Jennings, "Quantitative Design of SMIB Power System Stabilisers using Decoupling Theory", IFAC Proceedings Volumes, Volume 32, Issue 2, 1999, pp. 7382-7387.
- [4] Eduard Eitelberg, "Sampling rate design based on $(1 - sT/2)$ ". Int. J. Control, Vol. 48, No. 4, pp. 1423–1432.
- [5] Definition and classification of power system stability IEEE/CIGRE joint task force on stability terms and definitions, IEEE Transactions PWRs, Vol.19, No. 2, May 2004
- [6] IEEE Standard for Interconnection and Interoperability of Distributed Energy Resources with Associated Electric Power Systems Interfaces, IEEE Standards, IEEE 1547-2018.
- [7] Chris Greacen, Richard Engel, Thomas Quetchenbach, "A Guidebook on Grid Interconnection and Islanded Operation of Mini-Grid Power Systems Up to 200 kW", 2014
- [8] Israel Electric Corporation regulation, <https://www.iec.co.il/EN>
- [9] Bristol, E. H., 1966 "On a New Measure of Interaction of Multivariable Process Control", IEEE Trans. Autom. Control, AC-11, pp. 133-134.
- [10] Horowitz, Isaac, 1993, "Quantitative Feedback Design Theory (QFT)", QFT, Boulder.
- [11] Eduard Boje, 2002, "Multivariable Quantitative Feedback Design for Tracking Error Specifications", Automatica, 38, pp. 131-138.
- [12] Franklin, G. F., Powell, J. D., and Emami-Naeini, A., 1986, "Feedback control of Dynamic Systems"
- [13] Gupta, S. C., and Hasdorff, L., 1970, "Fundamentals of Automatic Control".
- [14] Eduard Eitelberg, "Control Engineering", NYOB, Durban.
- [15] Horowitz, I. M., and Liao, Y. K., 1986, Int. J. Control, 44, 663.
- [16] Hansen A. D., Sorenson P., Hansen L.H., Binder H., "models for a Stand-alone PV System", Riso-R-1219, 2001
- [17] Vincent Anayochukwu Ani, "Feasibility and Optimal Design of a Stand-Alone Photovoltaic Energy System for the Orphanage", *Journal of Renewable Energy*, vol. 2014, Article ID 379729, 8 pages, 2014.
- [18] Nayar, C.V. "Stand Alone Wind/Diesel/Battery Hybrid Energy Systems." *Wind Engineering*, vol. 21, no. 1, 1997, pp. 13–19.
- [19] Carvalho V.F, Power Plant Control' Ciger SC39/WG04 Survey Paper D, Ciger SC39/IFAC Meeting, Florence, September 1983.
- [20] IEEE Standards Board, Recommended Practice for Excitation System Models for Power System Stability Studies, IEEE Std. 421.1-1986
- [21] P.S. Rao, E.S. Boje, A quantitative design approach to PSS tuning, Electric Power Systems Research, 73 ,2005, p. 249–256.

- [22] Pretorius A., Boje E., “a complementary Quantitative Feedback Theory Solution to the 2×2 Tracking Error”, International Journal of Robust and Nonlinear Control, Vol. 30 Is. 16, pp. 6569-6584.
- [23] Eduard Eitelberg, “On Multi-loop interaction and relative and Bristol gains”, ASME journal of Dynamic Systems, Measurements and Control, Vol. 128, pp. 929-937, December 2006.
- [24] Eduard Eitelberg, “Considerate Control and Bristol Gains”, IEEE International Conference on the Science of Electrical Engineering in Israel (ICSEE), pp.1-5, 2018.
- [25] Eduard Eitelberg, Fadi Shakkour, “Control Configuration for an Experimental Turbo-Generator”, Mediterranean Conference on Control and Automation (MED), pp. 458-462, doi: 10.1109/MED.2019.8798524.
- [26] Y. S. H. Najjar, "Performance of Single-Cycle Gas Turbine Engines in Two Modes of Operation," Energy Conversion and Management, vol. 35, no. 5, pp. 433-441, 1994.
- [27] L. N. Hannett, G. Jee and B. Fardanesh, "A Governor/Turbine Model for a Twin-Shaft Combustion Turbine," IEEE Transactions on Power Systems, vol. 10, no. 1, pp. 133-140, 1995.
- [28] S. K. Yee, J. V. Milanovic´ and F. M. Hughes, "Overview and Comparative Analysis of Gas Turbine Models for System Stability Studies," IEEE Transactions on Power Systems, vol. 23, no. 1, pp. 108-118, 2008.
- [29] S. K. Yee, J. V. Milanovic´ and F. M. Hughes, "Validated Models for Gas Turbines Based on Thermodynamic Relationships," IEEE Transactions on Power Systems, vol. 26, no. 1, pp. 270-281, 2011.
- [30] R. Singh, A. Maity, P.S.V Natraj, “Shaft Speed Control of Laboratory Gas Turbine Engine”, IFAC-PaperOnline, vol. 52, no 12, pp. 262-267, 2019
- [31] <https://www.eskom.co.za/eskom-divisions/gx/peaking-power-stations/>
- [32] Dr. Daniel Kotek, private communication, 2016.
- [33] F Greg Shinskey , “Process control systems”, Third Edition. McGraw-Hill, Inc., pp.136, 1988
- [34] <https://www.sustainable.org.za/uploads/files/file49.pdf>
- [35] PJRC, Electronic Projects, <https://www.pjrc.com/>
- [36] Paul Breeze, “Power Generation Technologies (Third Edition)”, Newnes, 19